



Numerical Methods for Solving the Oblique Derivative Boundary Value Problems in Geodesy

Róbert Čunderlík, Marek Macák, Matej Medl'a, Karol Mikula,
and Zuzana Minarechová

Contents

1	Introduction	3
2	Formulation of the Oblique Derivative Boundary Value Problem	4
3	Numerical Solution by the Boundary Element Method	6
3.1	Boundary Integral Equation for the Fixed Gravimetric BVP	6
3.2	Collocation with Linear Basis Function	8
3.3	Numerical Experiments	13
4	Numerical Solution by the Finite Volume Method	15
5	The Oblique Derivative Boundary Condition in the Oblique Derivative Boundary Value Problem	17
5.1	Approach Based on the Central Scheme Applied on Uniform Grids	17
5.2	Approach Based on the First Order Upwind Scheme Applied on Uniform Grids	22
5.3	Approach Based on the Higher Order Upwind Scheme Applied on Non-uniform Grids	26
5.4	Controlling the Quality of Grid by Using the Tangential Redistribution of Points	27
5.5	Numerical Approximation of Evolving Surface	30
5.6	Discretization of the Oblique Derivative BVP for the Laplace Equation	35
5.7	Numerical Experiments	41
6	Summary	45
	References	45

This chapter is part of the series *Handbuch der Geodäsie*, volume “Mathematical Geodesy/Mathematische Geodäsie”, edited by Willi Freeden, Kaiserslautern.

R. Čunderlík (✉) · M. Macák · M. Medl'a · K. Mikula · Z. Minarechová
Faculty of Civil Engineering, Department of Mathematics and Descriptive Geometry, Slovak
University of Technology, Bratislava, Slovakia
E-Mail: cunderli@svf.stuba.sk; macak@math.sk; medla@math.sk; mikula@math.sk;
minarechova@math.sk

Abstract

We present various numerical approaches for solving the oblique derivative boundary value problem. At first, we describe a numerical solution by the boundary element method where the oblique derivative is treated by its decomposition into the normal and tangential components. The derived boundary integral equation is discretized using the collocation technique with linear basis functions. Then we present solution by the finite volume method on and above the Earth's surface. In this case, the oblique derivative in the boundary condition is treated in three different ways, namely (i) by an approach where the oblique derivative is decomposed into normal and two tangential components which are then approximated by means of numerical solution values (ii) by an approach based on the first order upwind scheme; and finally (iii) by a method for constructing non-uniform hexahedron 3D grids above the Earth's surface and the higher order upwind scheme. Every of proposed approaches is tested by the so-called experimental order of convergence. Numerical experiments on synthetic data aim to demonstrate their efficiency.

Zusammenfassung

Der Beitrag beschäftigt sich mit verschiedenen numerischen Verfahren zum schiefachsigen Randwertproblem der Geodsie. Zunächst wird eine numerische Lösung des Randwertproblems mittels Randelementmethoden beschrieben, welche die schiefachsigen Ableitungen in Normal- und Tangentialkomponenten zerlegt. Die sich ergebende Randintegralgleichung wird mittels Kollokationstechnik unter Verwendung linearer Basisfunktionen diskretisiert. Es folgt ein Lösungsvorschlag mittels Finite-Volumen-Technik auf und oberhalb der Erdoberfläche. In diesem Fall wird eine schiefachsige Ableitung auf drei verschiedene Arten behandelt, nämlich (i) durch einen Zerlegungsansatz in Normal- und zwei Tangentialkomponenten, die dann mittels numerischer Lösungswerte Approximation finden (ii) durch einen Zugang, der auf ein erster und zweiter Ordnung basierendes upwind – Schema umsetzt (iii) durch eine Methodik der Konstruktion nicht-gleichförmiger hexaedrischer 3D-Gitter oberhalb der Erdoberfläche und einem upwind Schema höherer Ordnung. Jeder der vorgeschlagenen Zugänge wird numerisch auf ihre Effizienz untersucht.

Keywords

Geodetic boundary value problem · Oblique derivative boundary condition · Boundary element method · Finite volume method · Numerical solution · Global gravity field modelling · Local gravity field modelling · Upwind method · Advection equation · Evolving surfaces

1 Introduction

A determination of the Earth's gravity field is usually formulated in terms of the geodetic boundary value problems (BVPs). A combination of terrestrial gravimetric measurements and precise 3D positioning by GNSS directly yields gravity disturbances. They naturally lead to boundary conditions (BC) of the fixed gravimetric boundary value problem (FGBVP), namely to the oblique derivative BC. Hence, from the mathematical point of view, the FGBVP represents an exterior oblique derivative geodetic BVP for the Laplace equation, cf. Koch and Pope [33], Freeden and Kersten [19], Bjerhammar and Svensson [8], Holota [28].

Classically, a solution procedure for the oblique derivative problem has been based on integral equations using the single-layer potential, cf. Bitzadse [7], Miranda [49]. Koch and Pope [33] applied such an integral equation procedure to solve the FGBVP. However, the strong nature of the singularities demanding Cauchy's principal integral values turned out to be a serious obstacle, see Freeden and Gerhards [18]. Later, Freeden and Kersten [20] proposed a new concept of approximations using the generalized Fourier expansions to transfer strongly singular integrals into regular ones and this approach has been further developed, e.g., in Freeden [17], Bauer [5], Gutting [24–26], Freeden and Michel [21], Freeden and Gerhards [18]. Recently, Freeden and Nutz [22] published the conceptual setup of the Runge-Walsh theorem for the oblique derivative problem of physical geodesy.

A development of high performance computing facilities has brought new opportunities for numerical solutions of the geodetic BVPs as well. Efficient numerical methods such as the boundary element method (BEM), the finite element method (FEM) or the finite volume method (FVM) can be also applied for global as well as local gravity field modelling. Among various approaches, we distinguish between solution to geodetic BVPs on infinite domains, see e.g., Holota [28], Klees et al. [32], Nesvadba et al. [50], Čunderlík et al. [11], Holota and Nesvadba [29], and on finite domains, cf. Fašková et al. [16], Minarechová et al. [48], Macák et al. [38].

In the case of BEM, there have been published several papers and here we mention only few of them, i.e., Klees [31], Lehmann and Klees [35], Klees et al. [32], Čunderlík et al. [11] or Čunderlík and Mikula [12]. The oblique derivative problem treated by BEM is discussed in Čunderlík et al. [13]. The FEM applied to gravity field modelling has been studied in Meissl [45], Shaofeng and Dingbo [53] or Fašková et al. [16]. The first application of FVM has been introduced by Fašková [15] and its parallel implementation by Minarechová et al. [48]. However, both papers have studied the geodetic BVP with the Neumann BC. The first insight of FVM applied to the oblique derivative BVP has been discussed in [39]. Later this effort was further developed in Macák et al. [38, 40], where treatment of the oblique derivative by the central scheme and the first order upwind scheme [36], respectively, were developed for solving FGBVPs on uniform grids above the ellipsoid. Recently, Medřa et al. [44] presented the FVM on non-uniform grids, where a discretization method based on an evolution of the Earth's surface has been developed. In this way, one obtains a more regular non-uniform 3D hexahedron grid.

Numerically, an innovative higher order upwind method for non-uniform grids has been applied.

In this chapter, we formulate the oblique derivative BVP and present concise solutions by two numerical methods, namely

- the boundary element method,
- the finite volume method.

In case of the BEM, the oblique derivative in the BC is decomposed into one normal and two tangential components that are expressed through the gradients of the unknown disturbing potential.

In case of the FVM, the oblique derivative in the BC is treated in three different ways, i.e.,

- the oblique derivative is decomposed into normal and two tangential components which are then approximated by means of numerical solution values using the central scheme applied on uniform grids,
- using the first order upwind scheme that is applied on uniform grids,
- using the higher order upwind scheme that is applied on non-uniform grids.

Every proposed approach is tested by various representative numerical experiments.

2 Formulation of the Oblique Derivative Boundary Value Problem

Let us consider the FGBVP, cf. [8, 28, 33]:

$$\Delta T(\mathbf{x}) = 0, \quad \mathbf{x} \in R^3 - S, \quad (1)$$

$$\nabla T(\mathbf{x}) \cdot \mathbf{s}(\mathbf{x}) = -\delta g(\mathbf{x}), \quad \mathbf{x} \in \partial S, \quad (2)$$

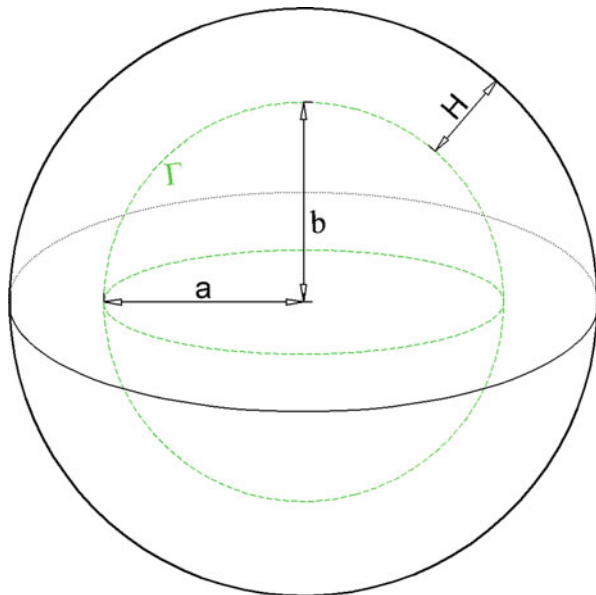
$$T(\mathbf{x}) \rightarrow 0, \quad \text{as } |\mathbf{x}| \rightarrow \infty, \quad (3)$$

where S is the Earth, $T(\mathbf{x})$ is the disturbing potential defined as a difference between the real and normal gravity potential at any point $\mathbf{x} = (x, y, z)$, $\delta g(\mathbf{x})$ is the gravity disturbance and $\mathbf{s}(\mathbf{x}) = -\nabla U(\mathbf{x})/|\nabla U(\mathbf{x})|$ is the unit vector normal to the equipotential surface of the normal potential $U(\mathbf{x})$ at any point \mathbf{x} .

Equations (1), (2), and (3) represent an exterior BVP for the Laplace equation, i.e., the computational domain (outside the Earth) is infinite. From the aforementioned numerical methods it is natural to apply BEM that is suitable for exterior BVPs since it reduces the problem from the 3D infinite domain onto its “2D” boundary.

On the contrary, FVM requires a discretization of the whole computational domain into finite volumes. To that goal we construct a domain Ω in the external space above the Earth, see [16]. Such a domain Ω (Fig. 1) is bounded by the bottom

Fig. 1 The bounded domain Ω – global gravity field modelling



surface $\Gamma \subset \partial\Omega$ representing the Earth’s surface and an upper surface created at appropriate altitude, e.g., at mean altitude of the GOCE satellite orbits.

In case of local gravity field modelling, see Fig. 2, we choose part of the Earth’s surface and we add side boundaries. Then on the top and side boundaries the Dirichlet-type BC for disturbing potential can be generated from any GOCE-based satellite-only geopotential model.

In the bounded domain Ω , we consider the following BVP

$$\Delta T(\mathbf{x}) = 0, \quad \mathbf{x} \in \Omega \subset \mathbb{R}^3, \tag{4}$$

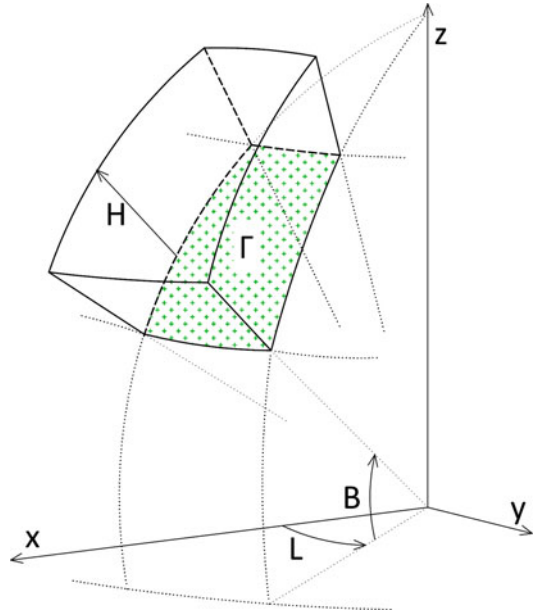
$$\nabla T(\mathbf{x}) \cdot \mathbf{s}(\mathbf{x}) = -\delta g(\mathbf{x}), \quad \mathbf{x} \in \Gamma \subset \partial\Omega, \tag{5}$$

$$T(\mathbf{x}) = T_{SAT}(\mathbf{x}), \quad \mathbf{x} \in \partial\Omega - \Gamma, \tag{6}$$

where $\Gamma \subset \partial\Omega$ represents the Earth topography or its part, i.e., the bottom boundary, $\partial\Omega - \Gamma$ represents the top boundary together with side boundaries (in case of local gravity field modelling), and T_{SAT} is the disturbing potential generated from any GOCE-based satellite-only geopotential model.

In the case that the Dirichlet and oblique derivative BC are obtained from different sources, problem with a compatibility of BC can arise on the edge where bottom and side boundaries meet. Then the Dirichlet BC (6) is prescribed also in a narrow band of the bottom boundary along to this edge, i.e., Γ is given by the bottom part of $\partial\Gamma$ minus the narrow band.

Fig. 2 The bounded domain
 Ω – local gravity field
 modelling



3 Numerical Solution by the Boundary Element Method

An objective of the BEM is to replace a partial differential equation solved in a 3D domain by an equivalent equation that gives a solution on the boundary of the domain only (cf. [9, 27, 37, 52]). There are two fundamental approaches to derive an integral formulation of the Laplace equation on the boundary. The first one is often called the direct method, i.e., the integral equations can be derived through an application of the Green's third identity. The second one is called the indirect method and is based on the assumption that harmonic functions can be expressed in terms of a single-layer or double-layer potential generated by continuous source density functions defined on the boundary. However, such source densities have usually formal character without a direct physical relation to the problem. Therefore in the following we focus on the direct BEM formulation where values of the function and its normal derivative over the boundary play the role of the source densities in generating the harmonic function over the whole solution domain [9].

3.1 Boundary Integral Equation for the Fixed Gravimetric BVP

A main advantage of BEM is the fact that only the boundary of the solution domain requires a division into its elements (Fig. 3), so the dimension of the problem is reduced by one. The direct BEM formulation applied to the Laplace equation (1) results in the boundary integral equation (BIE), [9]

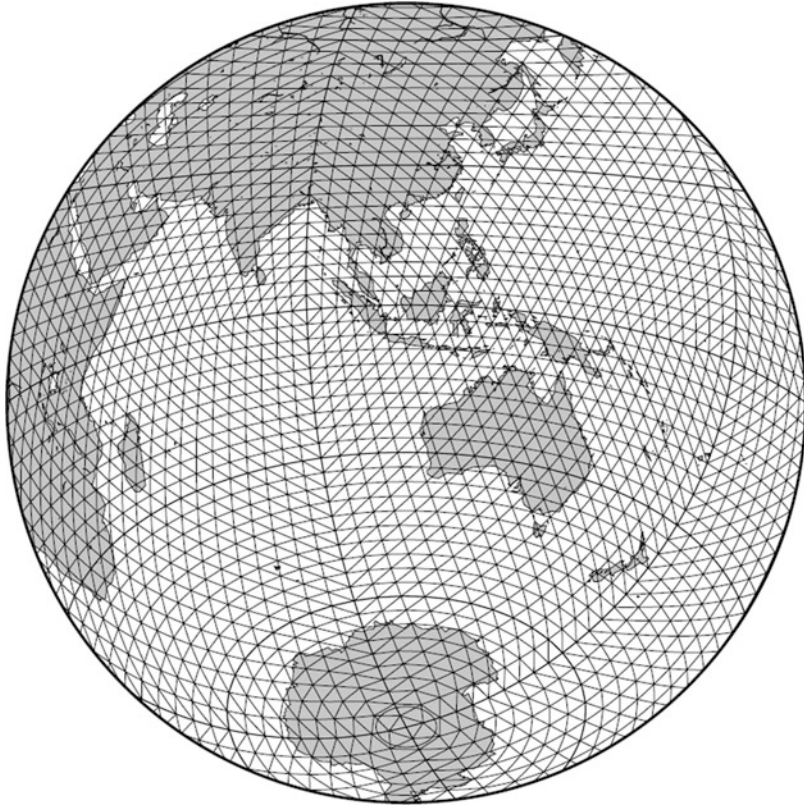


Fig. 3 The discretization of the Earth's surface by the global triangulation

$$\frac{1}{2}T(\mathbf{x}) + \int_{\Gamma} T(\mathbf{y}) \frac{\partial G}{\partial n}(\mathbf{x}, \mathbf{y}) d\mathbf{y} \Gamma = \int_{\Gamma} \frac{\partial T}{\partial n}(\mathbf{y}) G(\mathbf{x}, \mathbf{y}) d\mathbf{y} \Gamma, \quad (7)$$

where Γ is the boundary, $d\Gamma$ is the area element and the kernel function G represents the fundamental solution of the Laplace equation,

$$G(\mathbf{x}, \mathbf{y}) = \frac{1}{4\pi|\mathbf{x} - \mathbf{y}|}, \quad \mathbf{x}, \mathbf{y} \in R^3. \quad (8)$$

The term $\partial T/\partial n$ in BIE (7) represents the normal derivative, while FGBVP includes the oblique derivative BC. In order to derive BIE (7) for the oblique derivative problem we follow the idea described in [3]. At first we decompose the vector ∇T into the normal and tangential components

$$\nabla T = (\nabla T \cdot \mathbf{n})\mathbf{n} + (\nabla T \cdot \mathbf{t})\mathbf{t} + (\nabla T \cdot \mathbf{f})\mathbf{f}, \quad (9)$$

where \mathbf{n} is the unit normal vector, \mathbf{t} and \mathbf{f} are the unit tangential vectors. They represent a local orthonormal base system. Then the oblique derivative term can be written in the form

$$\nabla T \cdot \mathbf{s} = (\nabla T \cdot \mathbf{n})\mathbf{n} \cdot \mathbf{s} + (\nabla T \cdot \mathbf{t})\mathbf{t} \cdot \mathbf{s} + (\nabla T \cdot \mathbf{f})\mathbf{f} \cdot \mathbf{s}. \quad (10)$$

From this equation we express the normal derivative

$$\frac{\partial T}{\partial n} = \nabla T \cdot \mathbf{n} = \frac{1}{\mathbf{n} \cdot \mathbf{s}} [\nabla T \cdot \mathbf{s} - (\nabla T \cdot \mathbf{t})\mathbf{t} \cdot \mathbf{s} - (\nabla T \cdot \mathbf{f})\mathbf{f} \cdot \mathbf{s}]. \quad (11)$$

Inserting Eq. (11) into Eq. (7) we get BIE for our oblique derivative problem

$$\begin{aligned} \frac{1}{2}T(\mathbf{x}) + \int_{\Gamma} T(\mathbf{y}) \frac{\partial G}{\partial \mathbf{n}}(\mathbf{x}, \mathbf{y}) d_y \Gamma + \int_{\Gamma} \frac{((\nabla T \cdot \mathbf{t})\mathbf{t} \cdot \mathbf{s})}{(\mathbf{n} \cdot \mathbf{s})}(\mathbf{y}) G(\mathbf{x}, \mathbf{y}) d_y \Gamma + \\ + \int_{\Gamma} \frac{((\nabla T \cdot \mathbf{f})\mathbf{f} \cdot \mathbf{s})}{(\mathbf{n} \cdot \mathbf{s})}(\mathbf{y}) G(\mathbf{x}, \mathbf{y}) d_y \Gamma = \int_{\Gamma} \frac{(\nabla T \cdot \mathbf{s})}{(\mathbf{n} \cdot \mathbf{s})}(\mathbf{y}) G(\mathbf{x}, \mathbf{y}) d_y \Gamma, \quad \mathbf{x} \in \Gamma. \end{aligned} \quad (12)$$

The term $\nabla T \cdot \mathbf{s}$ on the right-hand side of BIE (12) represents the oblique derivative BC (2) and thus can be replaced by negative values of the input surface gravity disturbances. Then BIE (12) represents the direct BEM formulation for FGBVP defined by Eqs. (1), (2), and (3).

3.2 Collocation with Linear Basis Function

As a numerical technique to discretize BIE (12) we use the collocation method with linear basis functions (denoting by the C^1 collocation). The Earth's surface as a boundary of the domain is approximated by a triangulation of the topography expressed as a set of panels $\Delta\Gamma_j$ (Fig. 3), i.e., $\Gamma = \bigcup_{j=1}^N \Delta\Gamma_j$. The vertices

x_i, \dots, x_N of the triangles represent the nodes – the collocation points. The C^1 collocation involves a piecewise linear representation of the boundary functions T and δg on planar triangles [9]

$$T(\mathbf{x}) \approx \sum_{k=1}^3 T_k \psi_k(\mathbf{x}), \quad \mathbf{x} \in \Delta\Gamma_j, \quad (13)$$

$$\delta g(\mathbf{x}) \approx \sum_{k=1}^3 \delta g_k \psi_k(\mathbf{x}), \quad \mathbf{x} \in \Delta\Gamma_j, \quad (14)$$

where T_k and δg_k for $k = 1, 2, 3$ represent values of the boundary functions at the vertices of the triangle $\Delta\Gamma_j$. The linear basis functions $\psi_1, \psi_2, \dots, \psi_N$ are given by

$$\psi_j(\mathbf{x}_i) = 1, \quad \mathbf{x}_i = \mathbf{x}_j, \quad (15)$$

$$\psi_j(\mathbf{x}_i) = 0, \quad \mathbf{x}_i \neq \mathbf{x}_j, \quad (16)$$

where $i = 1, \dots, N$; $j = 1, \dots, N$ and N is the number of the collocation points. These approximations allow to reduce the original BIE (7) to a discrete form (more details can be found in [11]).

In the case of BIE (12) for the oblique derivative, a contribution of the tangential components is expressed through the gradients of the unknown disturbing potential. In the C^1 collocation they can be expressed through the gradients of the linear basis functions

$$\nabla T(\mathbf{x}) \approx \sum_{k=1}^3 T_k \nabla \psi_k(\mathbf{x}), \quad \mathbf{x} \in \Delta\Gamma_j, \quad (17)$$

where T_k are unknown values of the disturbing potential at collocation points that represent vertices of the triangle $\Delta\Gamma_j$ and ψ_k are the linear basis functions at these points. Since the gradient of the linear basis function $\nabla \psi_j$ is constant on the whole triangle $\Delta\Gamma_j$, it can be expressed using the Green theorem

$$\nabla \psi_j = \frac{1}{m(\Delta\Gamma_j)} \int_{\Delta\Gamma_j} \nabla \psi_j d\Delta\Gamma = \frac{1}{m(\Delta\Gamma_j)} \int_{\partial\Gamma_j} \psi_j \boldsymbol{\eta} d\partial\Gamma, \quad (18)$$

where $m(\Delta\Gamma_j)$ is the area of the triangle $\Delta\Gamma_j$ and $\boldsymbol{\eta}$ is the normal vector to its sides $\partial\Gamma$. Considering a fact that the j^{th} linear basis function equals to 1 at the j^{th} collocation point and to 0 at others vertices of the triangle $\Delta\Gamma_j$, i.e., at m^{th} and k^{th} collocation points, Eq. (17) can be simplified into the form

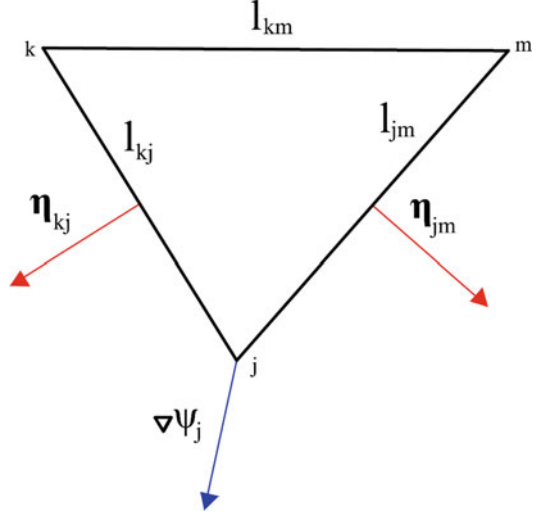
$$\nabla \psi_j = \frac{1}{2m(\Delta\Gamma_j)} [l_{jm} \boldsymbol{\eta}_{jm} + l_{jk} \boldsymbol{\eta}_{jk}], \quad (19)$$

where l_{jm} and l_{jk} are the lengths of the sides of the triangle intersecting at the j^{th} collocation point, and $\boldsymbol{\eta}_{jm}$ and $\boldsymbol{\eta}_{jk}$ are the normal vectors to these sides, see Fig. 4.

Considering all these approximations we get a discrete form of BIE (12) for each collocation point i .

$$c_i T_i \psi_i + \sum_{j=1}^N \int_{\text{supp}\psi_j} T_j \left[\frac{\partial G_{ij}}{\partial n} \psi_j + (\nabla \psi_j \cdot \mathbf{t}_j) \frac{s_j \cdot \mathbf{t}_j}{n_j \cdot s_j} G_{ij} + (\nabla \psi_j \cdot \mathbf{f}_j) \frac{s_j \cdot \mathbf{f}_j}{n_j \cdot s_j} G_{ij} \right] d\Gamma_j =$$

Fig. 4 Triangle intersecting at the j^{th} collocation point and normal vectors $\boldsymbol{\eta}_{jm}$ and $\boldsymbol{\eta}_{kj}$ to its sides



$$= \sum_{j=1}^N \int_{\text{supp}\psi_j} \delta g_j G_{ij} \frac{\psi_j}{n_j \cdot s_j} d\Gamma_j, \quad i = 1, \dots, N, \quad (20)$$

where $\text{supp}\psi_j$ is the support of the j^{th} basis function. The coefficient c_i represents a “spatial segment” bounded by the triangles joined at the i^{th} collocation point. In the case of the linear basis functions, it can be evaluated by the expression [42]

$$c_i = \frac{1}{4\pi} [2\pi + \sum_{s=1}^S \text{sgn}(\rho_i \cdot (n_s \times n_{s+1})) \arccos(n_s \cdot n_{s+2})], \quad (21)$$

where ρ_i is the distance vector at the i^{th} collocation point, n_s is the normal unit vector to the s^{th} triangle of the $\text{supp}\psi_i$ and S represents the number of triangles in the $\text{supp}\psi_i$.

Equations (20) represent the system of linear equations that can be rewritten into the matrix-vector form

$$\mathbf{M}\mathbf{t} = \mathbf{L}\boldsymbol{\delta g}, \quad (22)$$

where $\mathbf{t} = (T_1, \dots, T_N)^T$ and $\boldsymbol{\delta g} = (\delta g_1, \dots, \delta g_N)^T$. Coefficients of the matrices \mathbf{M} and \mathbf{L} represent integrals that need to be computed using an appropriate discretization of the integral operators in (20). The discretization of the integral operators is affected by the weak singularity of the kernel functions. The integrals with regular integrands, which represent non-diagonal coefficients, are approximated by the Gaussian quadrature rules defined on a triangle [34]. Their discrete form is given by

$$L_{ij} = \frac{1}{4\pi} \sum_{s=1}^S \frac{A_{j_s}}{\cos \varphi_{j_s}} \sum_{k=1}^K \frac{\psi_k w_k}{r_{ik_s}}, \quad i \neq j \quad (23)$$

$$M_{ij} = \frac{1}{4\pi} \sum_{s=1}^S \left[A_{j_s} \left(k_{ij_s} \sum_{k=1}^K \frac{\psi_k w_k}{r_{ik_s}^3} + \frac{\nabla \psi_{j_s} \cdot \mathbf{t}_j + \nabla \psi_{j_s} \cdot \mathbf{f}_j}{\cos \varphi_{j_s}} \sum_{k=1}^K \frac{w_k}{r_{ik_s}} \right) \right], \quad i \neq j \quad (24)$$

where A_{j_s} is the area of the s^{th} triangular element of the $\text{supp}\psi_j$, k_{ij_s} is the distance from the i^{th} collocation point to the plane represented by this triangular element, K is the number of points used for the Gaussian quadrature with their corresponding weights w_k and linear basis functions ψ_k , and r_{ik_s} is the distance from the i^{th} collocation point to the k^{th} quadrature point of the s^{th} triangular element. The j^{th} component of the vector $\delta \mathbf{g}$ in (22) corresponds to the input value of the measured surface gravity disturbance δg at the j^{th} collocation point. The $\cos \varphi_{j_s}$ represents a projection of the unit vector \mathbf{s} at the j^{th} collocation point to the normal vector \mathbf{n} of the s^{th} triangular element of the $\text{supp}\psi_j$, k_{ij_s} .

The non-regular integrals (singular elements) arise only for the diagonal components of the linear system. They require special evaluation techniques in order to handle the singularity of the kernel function. Thanks to the diagonal component c_i and the orthogonality of the normal to its planar triangular element, the singular element is represented by the spatial segment [3]

$$M_{ii} = c_i. \quad (25)$$

The kernel function G (Eq. (8)) in integrals on the right-hand side of Eq. (20) is weakly singular. Hence, the diagonal coefficients L_{ii} can be evaluated analytically

$$L_{ii} = \frac{1}{2\pi} \sum_{s=1}^S \frac{A_{i_s}}{\rho_s \cos \varphi_{i_s}} \ln \frac{\tan[(\beta_s + \alpha_s)/2]}{\tan(\beta_s/2)}. \quad (26)$$

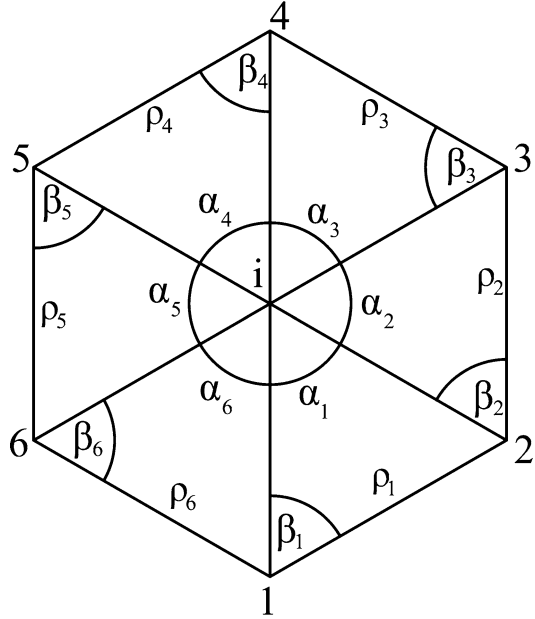
where A_{i_s} is the area of the s^{th} triangle of the $\text{supp}\psi_i$ determined by the line of length ρ_s and angles α_s , β_s (Fig. 5).

The diagonal component in Eq. (25) can be evaluated geometrically using (21) or through the physical consideration. The second approach is based on the fact that a constant potential applied over a closed body produces no flux. Accordingly, in case of the exterior Neumann problems, the sum of all components in each row should be equal to 1 [9]. Then one can easily calculate coefficient M_{ii} after evaluating of all non-diagonal coefficients, i.e.,

$$M_{ii} = 1 - \sum_{j=1, i \neq j}^N M_{ij}^*, \quad (27)$$

where coefficients M_{ij}^* do not include contributions of tangential components.

Fig. 5 Evaluating of the singular element (the C^1 collocation)



$$M_{ij}^* = \frac{1}{4\pi} \sum_{s=1}^S A_{js} k_{ijs} \sum_{k=1}^K \frac{\psi_k w_k}{r_{ik_s}^3}, i \neq j. \quad (28)$$

The matrix \mathbf{M} in Eq. (22) is a nonsymmetric dense $N \times N$ matrix. Consequently, memory requirements and CPU-time consumptions are of the order $O(N^2)$. It means that for increasing N (of the order 10^5 and more), the BEM applications lead to large-scale linear systems with enormous memory requirements. Therefore computing on parallel computers with distributed memory is practically inevitable.

In the last decades there have been developed numerous compression techniques that can be applied to reduce a numerical complexity of BEM, e.g., the fast multipole method (FMM), Hierarchical matrices (H-matrices) or panel clustering. Here we briefly mention that the FMM approximates the kernel function in Eq. (8) factorizing the \mathbf{x}, \mathbf{y} dependency by a multipole expansion [23]. Hence, interactions of the far zones can be evaluated straightforwardly and the original dense matrix \mathbf{M} is transformed into a sparse one. An implementation of the FMM as well as panel clustering to the gravity field modelling by the Galerkin BEM is published in [32].

A main idea of the H-matrices is based on an approximation of the entire system matrix that is split into a family of submatrices. Large submatrices are stored in factorized representation, while small submatrices are stored in standard representation. This allows to reduce memory requirements significantly while improving the efficiency. Among others we briefly mention the Adaptive Cross Approximation (ACA) algorithm where numerically rank-deficient sub-blocks, which correspond

to interactions of well-separated groups of nodes, can be efficiently compressed through an approach very similar to the column-pivoted LU decomposition [55].

3.3 Numerical Experiments

To demonstrate properties of our BEM approach, we present a reconstruction of a known harmonic function directly on the Earth’s surface where the corresponding oblique derivative BCs are prescribed. The Earth’s surface has been approximated by a triangulated surface. Vertices of the global triangulation have represented the collocation points and they have been regularly distributed over the whole Earth’s surface (Fig. 3). Their horizontal positions have been generated by the algorithm developed in [10]. A chosen level of the discretization has yielded a size of the triangular elements as well as number of collocation points (N) (Table 1). Vertical positions of the collocation points have been interpolated from the DNSC mean sea surface [1] at oceans, and SRTM30PLUS-V5.0 global topography model [6] on lands. In this way 3D positions of the collocation points have been constructed. At these points the disturbing potential as a reconstructed harmonic function and the surface gravity disturbances as the oblique derivative BCs have been generated from the EGM2008 geopotential model up to degree and order 2160 [51].

All large-scale parallel computations were performed on the cluster with 1.2 TB of distributed memory. The standard MPI (Message Passing Interface) subroutines [2] have been used for the code parallelization. As a linear solver, the BiConjugate Gradient Stabilized (BiCGSTAB) method [4, 54] has been used, which is suitable for dense and nonsymmetric matrices. To reduce large memory requirements we have used an iterative procedure introduced in [12]. In the first iterative step it has incorporated a priori known global solutions generated from the ITG-GRACE03S satellite-only geopotential model up to degree 180 [43]. These “approximate” values of the disturbing potential have been used to evaluate a contribution of the far zones to every collocation point. It means that all “far zones components” of the original system matrix multiplied by the approximate values of the unknown disturbing potential have been passed to the known right hand side of Eq. (22). In this way values of the disturbing potential at collocation points have been iteratively improved and the original dense stiffness matrix have been transformed into the

Table 1 Statistical characteristics of the residuals between the BEM solutions and EGM2008 [units: m^2s^{-2}]

CASE	A	B
Resolution	0.075 deg	0.05 deg
Nodes	5 760 002	12 960 002
Mean	-1.315	-0.939
Max	1.216	0.084
Min	-13.145	-7.320
STD	1.033	0.564

sparse one. Such an approach has allowed us to reduce the memory requirements significantly, however, in the cost of large CPU-time consumption.

Our experiences have shown that our numerical scheme based on the discrete BIE (20) works well for solutions on coarse grids or triangulations. However, for very refined triangulation the system matrix \mathbf{M} has become worse conditioned and the BiCGSTAB has stopped converge, even using preconditioning. It is due to the fact that in areas of extremely complicated Earth's surface, the tangential components have become stronger, and taking into account that the kernel function for the tangential components is one order stronger than for the normal component ($O(r^{-1})$ vs. $O(r^{-2})$, see Eq. (24)), this has caused the worse conditioned system matrix. To overcome such a drawback we have decided to use an iterative approach in which the tangential components have remained on the right-hand-side

$$\begin{aligned} & \frac{1}{2}T^P(p) + \int_{\Gamma} T^P(q) \frac{\partial G}{\partial \mathbf{n}}(p, q) d\Gamma_q = \\ & = \int_{\Gamma} \frac{\nabla T \cdot \mathbf{s} - (\nabla T^{P-1} \cdot \mathbf{t})\mathbf{t} \cdot \mathbf{s} - (\nabla T^{P-1} \cdot \mathbf{f})\mathbf{f} \cdot \mathbf{s}}{\mathbf{n} \cdot \mathbf{s}}(q)G(p, q) d\Gamma_q \quad (29) \end{aligned}$$

where P is an iterative step. Since we have used the iterative approach also for the elimination of far zones' interactions, in the first iteration we have used the same disturbing potential generated from the ITG-GRACE03S model. It means that in one process such an iterative procedure has treated both, the oblique derivative as well as elimination of far zones' interactions. Consequently, the system matrix has changed to \mathbf{M}^* which is generally well-conditioned also for refined triangulation and the BiCGSTAB solver has converged. Coefficients of the system matrix \mathbf{M}^* have been evaluated using Eqs. (27) and (28).

Table 1 summarizes statistical characteristics of the residuals between the BEM solutions and EGM2008 for different levels of the discretization. Figure 6 depicts these residuals. We remind that the BEM solutions are obtained at collocation points directly on the Earth's surface considering its complicated topography. It is evident that the largest residuals are in high mountains, especially in the Himalayas and Tibetan plateau. However, refining of the triangulation has resulted in an obvious improvement. This improvement has been achieved despite the fact that more refined triangulation has involved more detailed consideration of the Earth's surface topography. It is worth to note that the BEM applications allow also local refinements of the global triangulation. In this way one can achieve more precise solution, especially over regions with a complicated boundary, while the overall memory requirements can be reduced. And this is challenging for further investigation.

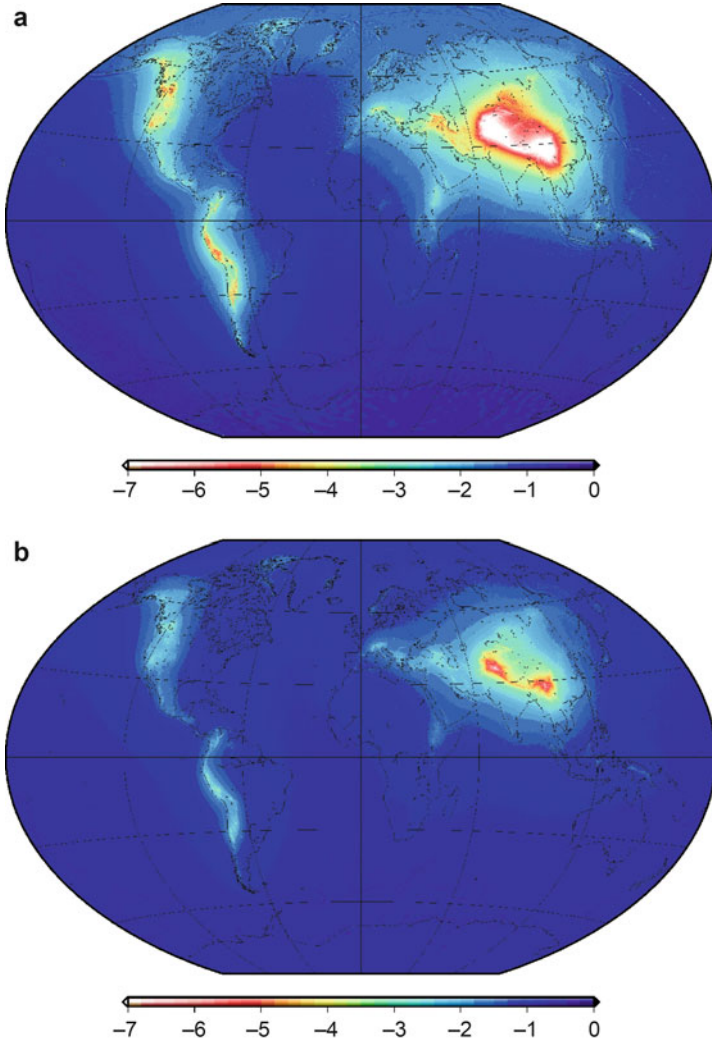


Fig. 6 Residuals between the BEM solution and EGM2008 for the triangulation with (a) 5 760 002, and (b) 12 960 002 collocation points [units: m^2s^{-2}]

4 Numerical Solution by the Finite Volume Method

The general discretization approach is to divide the computational domain Ω into the regular uniform hexahedron grid of finite volumes $V_{i,j,k}$. Then integrate the equation over each finite volume with a use of the divergence theorem that turns some of the volume integrals into surface integrals. Then the resulting discretised

equations equate fluxes across finite volumes to sources and sinks inside the volume, and they can be solved with standard direct or iterative methods.

So we multiply Eq. (4) by minus 1 and in aforementioned manner

$$- \int_{V_{i,j,k}} \Delta T \, dV = - \int_{\partial V_{i,j,k}} \nabla T \cdot \mathbf{n} \, dS. \quad (30)$$

we obtain the weak formulation of Eq. (4) in the finite volume $V_{i,j,k}$

$$- \int_{\partial V_{i,j,k}} \frac{\partial T}{\partial \mathbf{n}} \, dS = 0, \quad (31)$$

where \mathbf{n} is a unit normal vector to the boundary of the finite volume $V_{i,j,k}$.

Let us denote the representative point of the finite volume $V_{i,j,k}$ by $\mathbf{x}_{i,j,k}$. Finite volumes are constructed around inner (those that do not lie on the boundary $\partial\Omega$) representative points. Let N_1 denote the set of all triplets $(p, q, r), |p|+|q|+|r| = 1$. Then the finite volumes $V_{i+p,j+q,k+r}$, $(i, j, k) \in N_1$ share a common 2D boundary $e_{i,j,k}^{p,q,r}$ with the finite volume $V_{i,j,k}$.

Using such a discretization we can write

$$- \sum_{(p,q,r) \in N_1} \int_{e_{i,j,k}^{p,q,r}} \frac{\partial T}{\partial \mathbf{n}_{i,j,k}^{p,q,r}} \, dS = 0, \quad (32)$$

where $\mathbf{n}_{i,j,k}^{p,q,r}$ is the unit normal vector oriented from the finite volume $V_{i,j,k}$ to $V_{i+p,j+q,k+r}$. The derivation in the direction of the normal vector can be approximated by

$$\frac{\partial T}{\partial \mathbf{n}_{i,j,k}^{p,q,r}} \approx \frac{T_{i+p,j+q,k+r} - T_{i,j,k}}{d_{i,j,k}^{p,q,r}}. \quad (33)$$

Unknown values $T_{i,j,k}$ are considered in points $\mathbf{x}_{i,j,k}$ and $d_{i,j,k}^{p,q,r}$ is a distance between points $\mathbf{x}_{i,j,k}$ and $\mathbf{x}_{i+p,j+q,k+r}$. It is worth noting that the normal vector $\mathbf{n}_{i,j,k}^{p,q,r}$ has to be identical with the connecting line of representative points. In other case, the non-uniform grid has to be handled.

By considering the derivative in the normal direction to be constant on the boundary $e_{i,j,k}^{p,q,r}$ and utilizing Eq. (33) we obtain

$$- \sum_{(p,q,r) \in N_1} m \left(e_{i,j,k}^{p,q,r} \right) \frac{T_{i+p,j+q,k+r} - T_{i,j,k}}{d_{i,j,k}^{p,q,r}} = 0, \quad (34)$$

where $m\left(e_{i,j,k}^{p,q,r}\right)$ is an area of the boundary $e_{i,j,k}^{p,q,r}$. This equation can be written in the form

$$\sum_{(p,q,r) \in N_1} \frac{m\left(e_{i,j,k}^{p,q,r}\right)}{d_{i,j,k}^{p,q,r}} (T_{i,j,k} - T_{i+p,j+q,k+r}) = 0, \quad (35)$$

representing the linear system of algebraic equations for FVM. Then the term $\frac{m\left(e_{i,j,k}^{p,q,r}\right)}{d_{i,j,k}^{p,q,r}}$ defined on sides of the finite volume $V_{i,j,k}$ is referred to as the transmissivity coefficient [14]. The system (35) must be accompanied by BCs. In case of the Dirichlet BC (6), we prescribe the value of $T_{i+p,j+q,k+r}$ on the boundary. In case of the oblique derivative BC (5) it needs a special treatment which is discussed in the following section.

5 The Oblique Derivative Boundary Condition in the Oblique Derivative Boundary Value Problem

As we have mentioned above, in this section we present three different approaches to the oblique derivative BC in the oblique derivative BVPs, namely by

- (a) the central scheme applied on uniform grids,
- (b) the first order upwind scheme applied on uniform grids ,
- (c) the higher order upwind scheme applied on non-uniform grids .

5.1 Approach Based on the Central Scheme Applied on Uniform Grids

The following approximations apply for a finite volume $V_{i,j,k}$ for which the boundary $e_{i,j,k}^{-1,0,0}$ lies on the bottom boundary Γ (Fig. 7).

Let N_3 denote the set of all triplets (p, q, r) , $|p| + |q| + |r| = 3$. Then the finite volumes $V_{i+p,j+q,k+r}$, $(i, j, k) \in N_3$ share a common vertex with the finite volume $V_{i,j,k}$. Then let us denote this common vertex by $\mathbf{x}_{i,j,k}^{p,q,r}$ and it holds

$$\mathbf{x}_{i,j,k}^{p,q,r} = \frac{1}{8} \sum_{(l,m,n) \in B(p,q,r)} \mathbf{x}_{i+l,j+m,k+n}, \quad (36)$$

where

$$B(p, q, r) = \{(p, q, r), (p, q, 0), (p, 0, r), (p, 0, 0), (0, q, r), (0, q, 0), (0, 0, r), (0, 0, 0)\}.$$

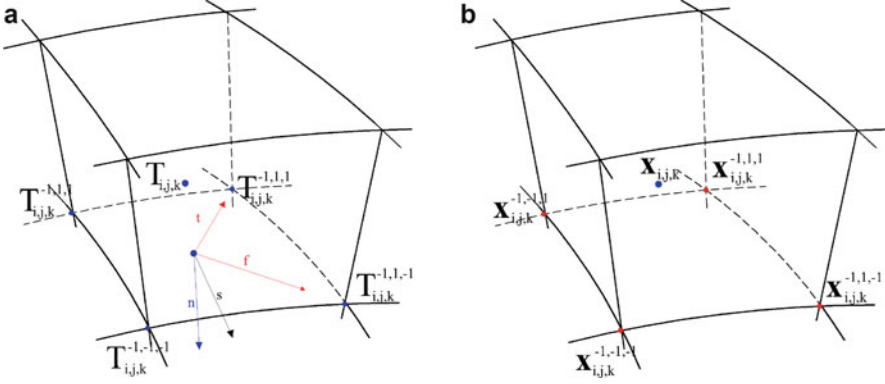


Fig. 7 Illustration of the FVM grid notation

So let us suppose the oblique derivative BVP (4), (5), and (6). We start by splitting the gradient in (5) into one normal and two tangential directions

$$\nabla T = (\nabla T \cdot \mathbf{n})\mathbf{n} + (\nabla T \cdot \mathbf{t})\mathbf{t} + (\nabla T \cdot \mathbf{f})\mathbf{f} = \frac{\partial T}{\partial \mathbf{n}}\mathbf{n} + \frac{\partial T}{\partial \mathbf{t}}\mathbf{t} + \frac{\partial T}{\partial \mathbf{f}}\mathbf{f}, \quad (37)$$

where \mathbf{n} is the normal vector and \mathbf{t} , \mathbf{f} are tangent vectors to $\Gamma \subset \partial\Omega \subset R^3$. These three vectors form an orthonormal basis. Then we put (37) into (5) to obtain

$$\nabla T \cdot \mathbf{s} = \left(\frac{\partial T}{\partial \mathbf{n}}\mathbf{n} + \frac{\partial T}{\partial \mathbf{t}}\mathbf{t} + \frac{\partial T}{\partial \mathbf{f}}\mathbf{f} \right) \cdot \mathbf{s} = \frac{\partial T}{\partial \mathbf{n}}\mathbf{n} \cdot \mathbf{s} + \frac{\partial T}{\partial \mathbf{t}}\mathbf{t} \cdot \mathbf{s} + \frac{\partial T}{\partial \mathbf{f}}\mathbf{f} \cdot \mathbf{s} \quad (38)$$

and the BC (5) is transformed into the form

$$\frac{\partial T}{\partial \mathbf{n}}\mathbf{n} \cdot \mathbf{s} + \frac{\partial T}{\partial \mathbf{t}}\mathbf{t} \cdot \mathbf{s} + \frac{\partial T}{\partial \mathbf{f}}\mathbf{f} \cdot \mathbf{s} = \delta g. \quad (39)$$

We set approximations of normal and tangent vectors

$$\begin{aligned} \mathbf{n} &= \frac{\mathbf{x}_{i-1,j,k} - \mathbf{x}_{i,j,k}}{|\mathbf{x}_{i-1,j,k} - \mathbf{x}_{i,j,k}|}, \\ \mathbf{t} &= \frac{\mathbf{x}_{i,j,k}^{-1,1,1} - \mathbf{x}_{i,j,k}^{-1,-1,-1}}{|\mathbf{x}_{i,j,k}^{-1,1,1} - \mathbf{x}_{i,j,k}^{-1,-1,-1}|}, \\ \mathbf{f} &= \frac{\mathbf{x}_{i,j,k}^{-1,1,-1} - \mathbf{x}_{i,j,k}^{-1,-1,1}}{|\mathbf{x}_{i,j,k}^{-1,1,-1} - \mathbf{x}_{i,j,k}^{-1,-1,1}|}. \end{aligned} \quad (40)$$

And we approximate the normal and tangential derivatives in (39) by

$$\begin{aligned}
\frac{\partial T}{\partial \mathbf{n}} &= \frac{T_{i-1,j,k} - T_{i,j,k}}{|\mathbf{x}_{i-1,j,k} - \mathbf{x}_{i,j,k}|}, \\
\frac{\partial T}{\partial \mathbf{t}} &= \frac{T_{i,j,k}^{-1,1,1} - T_{i,j,k}^{-1,-1,-1}}{|\mathbf{x}_{i,j,k}^{-1,1,1} - \mathbf{x}_{i,j,k}^{-1,-1,-1}|}, \\
\frac{\partial T}{\partial \mathbf{f}} &= \frac{T_{i,j,k}^{-1,1,-1} - T_{i,j,k}^{-1,-1,1}}{|\mathbf{x}_{i,j,k}^{-1,1,-1} - \mathbf{x}_{i,j,k}^{-1,-1,1}|},
\end{aligned} \tag{41}$$

where values $T_{i,j,k}^{p,q,r}$ are defined by

$$T_{i,j,k}^{p,q,r} = \frac{1}{8} \sum_{(l,m,n) \in B(p,q,r)} T_{i+l,j+m,k+n}, \tag{42}$$

If we put these approximations into (39) we get a discrete form of the 3D oblique derivative BC (5)

$$\begin{aligned}
\nabla T \cdot \mathbf{s} &\approx \frac{T_{i-1,j,k} - T_{i,j,k}}{|\mathbf{x}_{i-1,j,k} - \mathbf{x}_{i,j,k}|} \mathbf{n} \cdot \mathbf{s} + \frac{T_{i,j,k}^{-1,1,1} - T_{i,j,k}^{-1,-1,-1}}{|\mathbf{x}_{i,j,k}^{-1,1,1} - \mathbf{x}_{i,j,k}^{-1,-1,-1}|} \mathbf{t} \cdot \mathbf{s} + \\
&+ \frac{T_{i,j,k}^{-1,1,-1} - T_{i,j,k}^{-1,-1,1}}{|\mathbf{x}_{i,j,k}^{-1,1,-1} - \mathbf{x}_{i,j,k}^{-1,-1,1}|} \mathbf{f} \cdot \mathbf{s} = \delta g.
\end{aligned} \tag{43}$$

These equations are incorporated into the FVM linear system which is then solved.

5.1.1 Numerical Experiments

The numerical schemes will be qualified according to the value of the so-called experimental order of convergence (EOC) that can be computed as follows. If we assume that the error of the scheme in some norm is proportional to some power of the grid size, i.e., $Error(h) = Ch^\epsilon$, with a constant C , then having two grids with sizes h_1 and h_2 , where $h_1 > h_2$, yields two errors $Error(h_1) = C(h_1)^\epsilon$ and $Error(h_2) = C(h_2)^\epsilon$ from where we can simply extract $\epsilon = \log_{\frac{h_1}{h_2}}(Error(h_1)/Error(h_2))$. If $h_2 = \frac{h_1}{2}$ then $\epsilon = \log_2(Error(h_1)/Error(h_2))$. Then the ϵ is the EOC and can be determined by comparing numerical solutions and exact solutions on subsequently refined grids.

Now let us remind that gravity disturbance defined as a difference between magnitudes of the real and normal gravity represents a projection of $\nabla T(\mathbf{x})$ into the unit vector $\mathbf{s}(\mathbf{x})$. The oblique derivative arises from the fact that the direction of $\mathbf{s}(\mathbf{x})$ in general does not coincide with the normal $\mathbf{n}(\mathbf{x})$ to the Earth's surface. It means that here we can distinguish two angles; the first one between $\mathbf{n}(\mathbf{x})$ and $\mathbf{s}(\mathbf{x})$ is known, while the second one between $\nabla T(\mathbf{x})$ and $\mathbf{s}(\mathbf{x})$ is unknown due to an

unknown direction of $\nabla T(\mathbf{x})$. To simulate such a situation we perform the following two testing experiments.

In the first testing experiment, we have the computational domain a tesseroid bounded by two concentric spheres with radii $r_1 = 1$ and $r_2 = 2$, and a coaxial cone with dimension $(0, \pi/2) \times (0, \pi/2)$. There have been the oblique BC (5) on the bottom boundary and the Dirichlet BC on the upper and side boundaries applied. The oblique derivative vector \mathbf{s} is chosen to be

$$\mathbf{s} = \frac{\mathbf{x}_C - \mathbf{x}_{i-\frac{1}{2},j,k}}{|\mathbf{x}_C - \mathbf{x}_{i-\frac{1}{2},j,k}|},$$

where the center point is $\mathbf{x}_C = (0.1, -0.2, -0.1)$. As the Dirichlet BC (6) we have considered the exact solution of (4) in the form $\mathbf{T}(x, y, z) = 1/r$, where r is the distance from the center point \mathbf{x}_C . As the Neumann/oblique BC on the bottom boundary, we have supposed the derivative of this exact solution that is equal to $-1/r^2$. The results can be seen in Table 2. One can see that the proposed approach is second order accurate.

For the second testing experiment we have the same computational domain and the same BCs as in the previous one, but the oblique vector \mathbf{s} has been rotated by 20° . The coordinates of the center point have been $\mathbf{x}_C = (-0.2, 0.1, 0.2)$. The $L_2(\Omega)$ -norm of differences between the exact and numerical solutions as well as the EOC of the method are shown in Table 3. One can see that also in this case with the rotated oblique vector, the value of EOC of the proposed approach reaches value 2. It is worth noting that in case when the oblique vector is identical with gradient vector, we can project to the normal without incorporating error. However, if this is not so (this is the case of rotation), we can't solve BVP with Neumann BC, but we have to use the proposed approach.

The third numerical experiment has dealt with the FGBVP and the computational domain Ω above Himalaya region approximated by the ellipsoid WGS84. A

Table 2 The $L_2(\Omega)$ -norm and the EOC for the experiment with the oblique BC, when the center point is shifted $\mathbf{x}_C = (0.1, -0.2, -0.1)$

$n_1 \times n_2 \times n_3$	$\ \mathbf{T} - T\ _{L_2(\Omega)}$	EOC
$2 \times 2 \times 4$	$6.74805 \cdot 10^{-2}$	–
$4 \times 4 \times 8$	$9.00317 \cdot 10^{-3}$	2.90597
$8 \times 8 \times 16$	$1.54266 \cdot 10^{-3}$	2.54502
$16 \times 16 \times 32$	$3.01950 \cdot 10^{-4}$	2.35328
$32 \times 32 \times 64$	$0.67123 \cdot 10^{-5}$	2.16928

Table 3 The $L_2(\Omega)$ -norm and the EOC for the experiment with the oblique BC. The center point is shifted $\mathbf{x}_C = (-0.2, 0.1, 0.2)$ and the oblique vector \mathbf{s} is rotated by 20°

$n_1 \times n_2 \times n_3$	$\ \mathbf{T} - T\ _{L_2(\Omega)}$	EOC
$2 \times 2 \times 4$	$6.43828 \cdot 10^{-2}$	–
$4 \times 4 \times 8$	$8.14779 \cdot 10^{-3}$	2.98220
$8 \times 8 \times 16$	$1.34261 \cdot 10^{-3}$	2.60137
$16 \times 16 \times 32$	$2.44307 \cdot 10^{-4}$	2.45827
$32 \times 32 \times 64$	$0.52002 \cdot 10^{-5}$	2.23204

range for the ellipsoidal latitude and longitude has been $B \in \langle 20.0^\circ, 50.0^\circ \rangle$ and $L \in \langle 60.0^\circ, 110.0^\circ \rangle$, respectively. To calculate the oblique derivative vector, the ellipsoidal heights above reference ellipsoid WGS84 have been generated from SRTM30 [6]. The upper boundary has been 240 km above the WGS84 reference ellipsoid. The number of finite volumes has been 1200 in height, 900 in meridional and 1500 in zonal directions, i.e., $5' \times 5' \times 200$ m sized volumes have been created. All BCs, namely gravity disturbances as well the disturbing potential, have been generated from EGM2008, see [51]. Results are depicted in Figs. 8 and 9 with

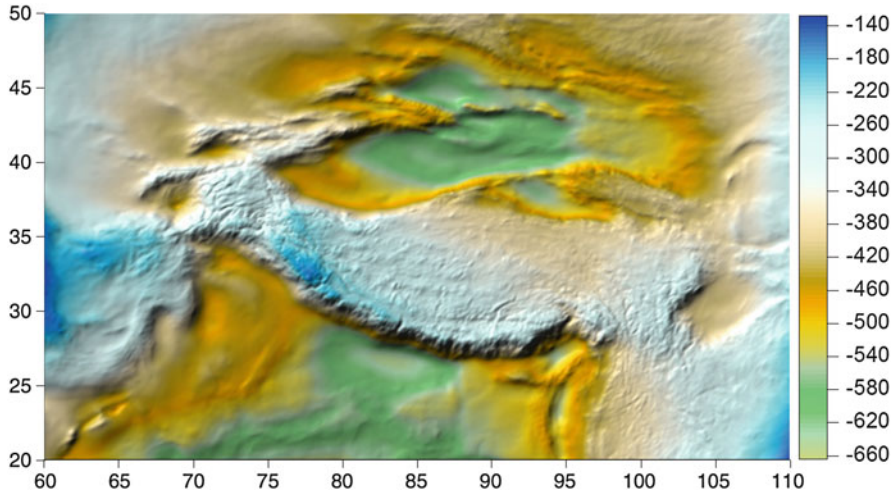


Fig. 8 The disturbing potential solution T in the area of Himalaya region [units: m^2s^{-2}]

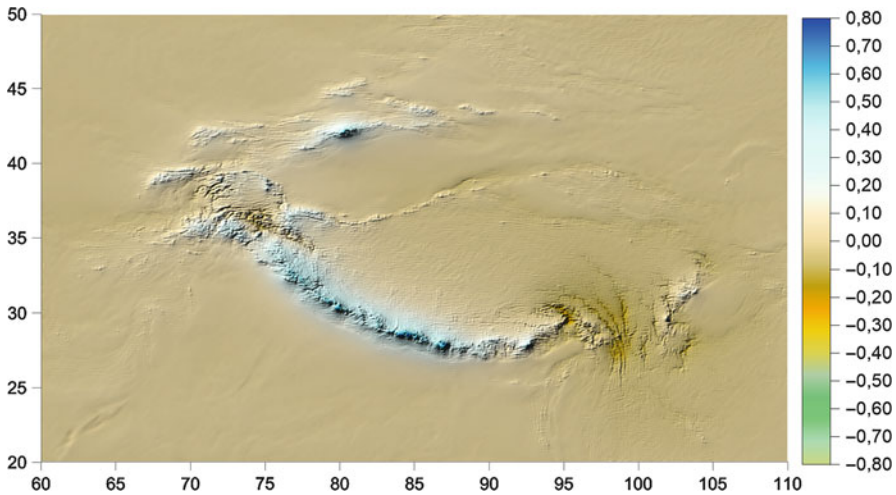
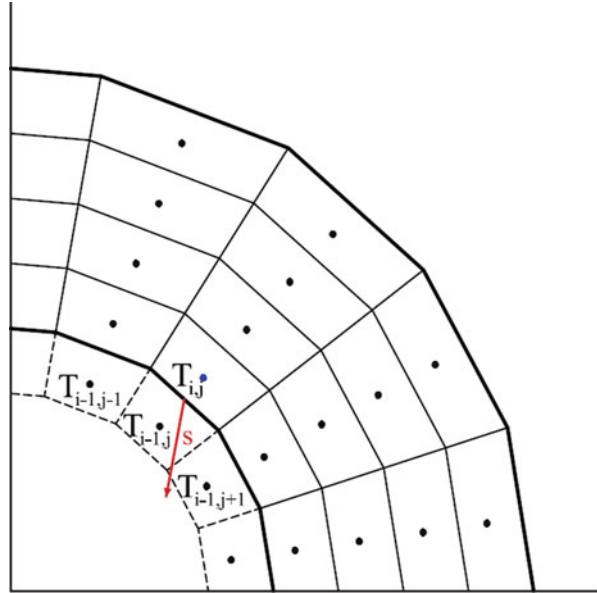


Fig. 9 Local improvement in T from the oblique BC when using EGM08 data only [units: m^2s^{-2}]

Table 4 Comparison of statistical characteristics in between the disturbing potential computed by FVM applied to solving BVP with the oblique BC using EGM08 data only, and the disturbing potential generated from EGM08 directly [units: m^2s^{-2}]

AREA	HIMALAYA
Min	-0.87
Mean	0.04
Max	0.95
Std	0.17
RMS	0.18

Fig. 10 Illustration of the 2D FVM grid. The dashed lines denote the boundaries of added finite volumes, the vector \mathbf{s} is depicted by red



corresponding statistics presented in Table 4. One can observe that the highest values of residuals are in the areas of the mountainous ridges.

More details about this approach can be found in [41].

5.2 Approach Based on the First Order Upwind Scheme Applied on Uniform Grids

In this approach, the oblique derivative BC is interpreted as a stationary advection equation for the unknown disturbing potential. Then its approximation is done by using the first order upwind scheme, which takes into account information from inflow parts of the finite volume boundary only.

Since in upwind scheme is natural to have outer normal to the computational domain (see Fig. 10), we multiply the unit vector $\mathbf{s}(\mathbf{x})$ by minus 1.

So one can rewrite the divergence of $T(\mathbf{x})\mathbf{s}(\mathbf{x})$ in the form

$$\nabla \cdot (T(\mathbf{x})\mathbf{s}(\mathbf{x})) = T(\mathbf{x})\nabla \cdot \mathbf{s}(\mathbf{x}) + \nabla T(\mathbf{x}) \cdot \mathbf{s}(\mathbf{x}). \quad (44)$$

By inserting (44) into Eq. (5), we obtain

$$\nabla \cdot (T(\mathbf{x})\mathbf{s}(\mathbf{x})) - T(\mathbf{x})\nabla \cdot \mathbf{s}(\mathbf{x}) = \delta g(\mathbf{x}). \quad (45)$$

We add one row of finite volumes under the bottom boundary, see Fig. 10, and integrate (45) over one of the added finite volumes $V_{i,j,k}$ (we omit (\mathbf{x}) to simplify the notation in the following equations)

$$\int_{V_{i,j,k}} \nabla \cdot (T\mathbf{s}) dV - \int_{V_{i,j,k}} T\nabla \cdot \mathbf{s} dV = \int_{V_{i,j,k}} \delta g dV. \quad (46)$$

Using a constant approximation of the solution T on the finite volume $V_{i,j,k}$ denoted by $T_{i,j,k}$ and applying the divergence theorem to the left-hand side of Eq. (46) we obtain

$$\begin{aligned} \sum_{(p,q,r) \in N_1} \int_{e_{i,j,k}^{p,q,r}} T \mathbf{s} \cdot \mathbf{n}_{i,j,k}^{p,q,r} dS - \sum_{(p,q,r) \in N_1} T_{i,j,k} \int_{e_{i,j,k}^{p,q,r}} \mathbf{s} \cdot \mathbf{n}_{i,j,k}^{p,q,r} dS = \\ = \int_{V_{i,j,k}} \delta g dV. \end{aligned} \quad (47)$$

Denoting a constant approximation of the solution on the interface $e_{i,j,k}^{p,q,r}$ by $T_{i,j,k}^{p,q,r}$ and a volume of the finite volume $V_{i,j,k}$ by $m(V_{i,j,k})$ yields

$$\begin{aligned} \sum_{(p,q,r) \in N_1} T_{i,j,k}^{p,q,r} \int_{e_{i,j,k}^{p,q,r}} \mathbf{s} \cdot \mathbf{n}_{i,j,k}^{p,q,r} dS - \sum_{(p,q,r) \in N_1} T_{i,j,k} \int_{e_{i,j,k}^{p,q,r}} \mathbf{s} \cdot \mathbf{n}_{i,j,k}^{p,q,r} dS \\ = \delta g m(V_{i,j,k}). \end{aligned} \quad (48)$$

When we denote

$$s_{i,j,k}^{p,q,r} = \int_{e_{i,j,k}^{p,q,r}} \mathbf{s} \cdot \mathbf{n}_{i,j,k}^{p,q,r} dS \approx m(e_{i,j,k}^{p,q,r}) \mathbf{s} \cdot \mathbf{n}_{i,j,k}^{p,q,r}, \quad (49)$$

we finally obtain

$$\sum_{(p,q,r) \in N_1} s_{i,j,k}^{p,q,r} (T_{i,j,k}^{p,q,r} - T_{i,j,k}) = \delta g m(p). \quad (50)$$

Due to an analogy of the oblique derivative BC (5) and the stationary advection equation, we have applied an upwind principle, which is used exclusively in solving advection equations in fluid dynamics [36]. Then we define

$$T_{i,j,k}^{p,q,r} = T_{i,j,k}, \quad \text{if } s_{i,j,k}^{p,q,r} > 0, \quad (51)$$

$$T_{i,j,k}^{p,q,r} = T_{i+p,j+q,k+r}, \quad \text{if } s_{i,j,k}^{p,q,r} < 0, \quad (52)$$

which correspond to the inflow part to the finite volume $V_{i,j,k}$ ($s_{i,j,k}^{p,q,r} < 0$) and outflow part to the finite volume $V_{i,j,k}$ ($s_{i,j,k}^{p,q,r} > 0$) when \mathbf{s} is understood as an advection velocity vector. By using (51) and (52) in (50) we obtain the final form of an approximation to the oblique derivative BC (5) as

$$\sum_{(p,q,r) \in N_1^{in}} s_{i,j,k}^{p,q,r} (T_{i+p,j+q,k+r} - T_{i,j,k}) = \delta g m(p), \quad (53)$$

where N_1^{in} is a set of neighbours at the inflow boundaries of the finite volume $V_{i,j,k}$, i.e., where $s_{i,j,k}^{p,q,r} < 0$.

5.2.1 Numerical Experiments

Now, we present two numerical experiments, one testing and one with real data. In the testing numerical experiment, the computational domain has been a tesseroid bounded by two concentric spheres with radii $R_d = 1$ m and $R_u = 2$ m, and a coaxial cone with dimension $(0, \pi/4) \times (0, \pi/4)$. As the Dirichlet BC (6), the exact solution of (5) in the form $T^* = 1/r$ on the upper and the side boundaries, has been prescribed. The direction of the unit vector $\mathbf{s}_1(\mathbf{x})$, i.e., the unit gradient vector of the exact solution, has been modified by angle $\pm\alpha$ to create a new unit vector $\mathbf{s}(\mathbf{x})$. For this experiment we have chosen $\alpha = 20^\circ$. The coordinates of the point mass source have been $\mathbf{x}_C = (0.3, -0.2, 0.1)$. Then the oblique derivative BC is given by the projection $\nabla T(\mathbf{x}) \cdot \mathbf{s}(\mathbf{x}) = -(1/r^2) \cos(\alpha)$. The $L_2(\Omega)$ and $MAX(\Gamma)$ norms of differences between the exact and numerical solutions and the EOC of the methods are shown in Table 5. We observe stable behaviour of EOC for the upwind scheme and oscillatory EOC for the central scheme.

Table 5 The $L_2(\Omega)$ -norm, $MAX(\Gamma)$ -norm and the EOC for the 3D experiment with the 3D oblique derivative BC when the oblique vector \mathbf{s} does not have direction of the solution gradient

$n_1 \times n_2 \times n_3$	Upwind scheme			Central scheme				
	$\ T^* - T\ _{L_2(\Omega)}$	EOC	$\ T^* - T\ _{MAX(\Gamma)}$	EOC	$\ T^* - T\ _{L_2(\Omega)}$	EOC	$\ T^* - T\ _{MAX(\Gamma)}$	EOC
$8 \times 8 \times 4$	0.177728	–	0.362022	–	0.061529	–	0.3511	–
$16 \times 16 \times 8$	0.059441	1.58	0.177806	1.03	0.146351	–1.25	0.209212	0.75
$32 \times 32 \times 16$	0.022542	1.39	0.083563	1.08	0.058753	1.31	0.050549	2.05
$64 \times 64 \times 32$	0.010819	1.05	0.041756	1.00	0.008090	2.86	0.053722	2.64
$128 \times 128 \times 64$	0.005143	1.07	0.019506	1.13	0.004520	0.83	0.024245	0.84

In numerical experiment with real data, we apply the upwind scheme for global gravity field modelling. We try to reconstruct a harmonic function given by the EGM2008 geopotential model up to degree 2160 [51]. It means that all BCs are generated from this model. The Dirichlet BC in the form of the disturbing potential is prescribed on the upper boundary at the constant altitude of 240 km above the reference ellipsoid. The oblique derivative BCs are generated as the first derivative of the disturbing potential in the direction of the normal to the reference ellipsoid. They are generated at points on the real topography that is approximated using the SRTM30PLUS global topography model [6]. Our goal is to show a convergence of the FVM solution to EGM2008 when refining the computational grid.

Although the oblique derivative BCs are considered at points on the real topography, in our FVM approach we so far use a structured grid of finite volumes. It means that the computational domain Ω in our computations is bounded by the reference ellipsoid. However, all input data here are adopted from the real topography. This means that $\mathbf{n}_{i,j,k}^{p,q,r}$ on the bottom boundary is given by the normal to the topography and not by the normal to the ellipsoid. Then the unit vector $\mathbf{s}(\mathbf{x})$ represents the normal to the reference ellipsoid while the direction of $\mathbf{n}_{i,j,k}^{p,q,r}$ represents the normal to the Earth’s surface and is adopted from our approximation of the topography. In this way we are able to evaluate the coefficients $s_{i,j,k}^{p,q,r}$ in our approximation of the oblique derivative BC.

The computational grid is constructed using the number of divisions in L, B, H directions given by $n_1 \times n_2 \times n_3$:

- (a) $540 \times 270 \times 75$ (resolution: $40' \times 40' \times 3200$ m),
- (b) $1080 \times 540 \times 150$ (resolution: $20' \times 20' \times 1600$ m),
- (c) $2160 \times 1080 \times 300$ (resolution: $10' \times 10' \times 800$ m),
- (d) $4320 \times 2160 \times 600$ (resolution: $5' \times 5' \times 400$ m).

The obtained FVM solutions are compared with EGM2008. The statistical characteristics of residuals on the bottom boundary as well as computational aspects are summarized in Table 6. One can see that the FVM solution converges to EGM2008 by refining the finite volume grid, i.e., the mean value, STD as well as maximum norm are decreasing. It is worth to note that every refinement of the discretization involves a more detailed consideration of the topography. This does not allow us to compute EOC directly, however, STD as well as the maximum norm in Table 6 indicate that the upwind scheme is the first order accurate.

Table 6 Statistics of residuals in $T[m^2s^{-2}]$ on the bottom boundary Γ for successive refinements, and computational details

Resolution	Min.	Max.	Mean	STD (total)	STD (Sea)	STD (Land)
$40' \times 40'$	-78.910	80.426	-0.392	5.238	4.771	6.228
$20' \times 20'$	-46.584	27.558	-0.273	1.948	1.489	2.750
$10' \times 10'$	-22.011	7.954	-0.265	0.904	0.327	1.578
$5' \times 5'$	-13.926	7.932	-0.114	0.558	0.183	0.991

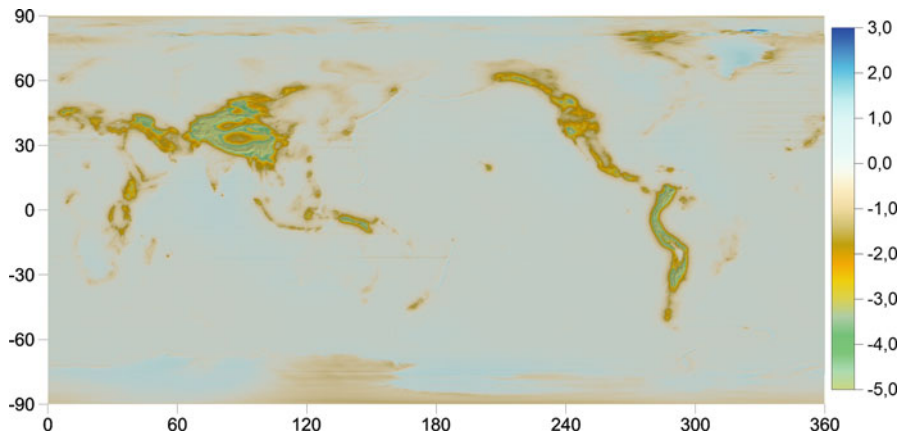


Fig. 11 Residuals in T [$m^2 \cdot s^{-2}$] between the disturbing potential computed by the FVM solution with upwind treatment of oblique derivative and EGM2008 solution on the bottom boundary Γ

The residuals between the most refined FVM solution in case (d) and EGM2008 are depicted in Fig. 11. The largest residuals are negative and they evidently correlate with high mountainous areas of Himalayas and Andes. The minimal values of residuals in Table 6 indicate that refinements of the discretization improve the FVM solution also in these zones of complicated topography. This confirms that the presented FVM approach based on the upwind treatment of the oblique derivative BC is able to reconstruct a harmonic function and thus is efficient to solve the oblique derivative BVP.

More details about this approach can be found in [38].

5.3 Approach Based on the Higher Order Upwind Scheme Applied on Non-uniform Grids

Now we will present FVM on non-uniform grids above the Earth's topography. The oblique derivative BC is again treated as a stationary advection equation. We use a method for discretization of the computational domain based on an evolution of the Earth's surface depending on its mean curvature. This approach involves a tangential redistribution of the evolving surface discretization points leading to a construction of a more regular non-uniform 3D hexahedron grid. Then we present a discretization of the Laplace equation and oblique derivative BC on such non-uniform grids. It consists of a reconstruction of the normal derivative to the finite volume using derivatives in the tangential directions. Numerically, the oblique derivative BC treated as an advection equation and a new higher order upwind method for non-uniform grids are applied.

First, let us see the computational domain Ω and its grid as a parametrized volume. A parametrization determines a distribution of points, which in a discrete

form determines our finite volume grid. Let us denote by $S = \{\mathbf{x}(u, v, t), u \in (0, 1), v \in (0, 1), t \in (0, t_{end})\}$ the unknown parametrization of Ω . We consider that $S(u, v, 0)$ approximates the Earth's topography and we would like to force it in such a way that $S(u, v, t_{end})$ forms approximately a part of an ellipsoid at height H above the reference ellipsoid. This problem can be treated in such a way that $S(u, v, t_{end})$ will be the reference ellipsoid, which is then scaled to be approximately at the height H and $S(u, v, 0)$ remains unchanged. The 3D volume S can be seen as an evolving surface for which parameter t is the time. The grid is constructed by an evolution of the surface $S(u, v, 0)$ by its mean curvature and a force f , where f corresponds to the mean curvature of the reference ellipsoid in the point S^* . The point S^* is given by the projection of $S(u, v, t)$ to the reference ellipsoid. Using this evolution we achieve that the surface continuously forms a shape of a part of the ellipsoid and the mathematical formulation of this process is given by [46]

$$\partial_t \mathbf{x}(u, v, t) = \varepsilon (k\mathbf{N} + f\mathbf{N}), \quad (54)$$

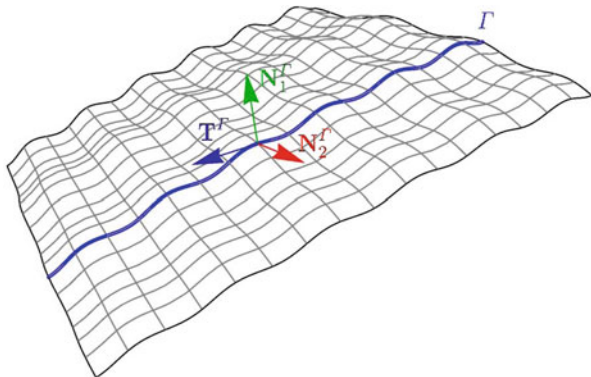
where unknown \mathbf{x} is the position vector of the evolving surface S , k is two times its mean curvature and \mathbf{N} is the normal vector at the point \mathbf{x} . The scalar f is the force applied in direction of the normal vector \mathbf{N} . The vector $k\mathbf{N}$ is computed as $k\mathbf{N} = \Delta_s \mathbf{x}$, where Δ_s is the so-called Laplace-Beltrami operator [46]. The scalar ε is a parameter determining how fast the surface is moving. The equation (54) is solved using the FVM. Boundary points of the surface do not have to be on the reference ellipsoid at time 0 due to real topography. We want them to get on the reference ellipsoid in time t_{end} . So we decided that boundary points will move linearly to the points on the ellipsoid, but we allow them also a tangential movement. Points of the grid of the computational domain Ω are discrete points of scaled S . These points are scaled around the origin $(0, 0, 0)$ with the factor $1 + 240000/6378137$.

5.4 Controlling the Quality of Grid by Using the Tangential Redistribution of Points

A redistribution of points on a surface is important for a uniformity of the computational grid and a numerical stability of a surface evolution. In our approach, we decided to follow principles published in [30, 46]. In this case, the discrete surface is composed by discrete parallels and meridians which cross in discrete points \mathbf{x}_{ij} . In the point \mathbf{x}_{ij} , the i -th discrete meridian crosses the j -th discrete parallel. Then the uniform redistribution can be achieved by adding a tangential movement of the surface in the directions \mathbf{T}^{pi} and \mathbf{T}^{mj} , where \mathbf{T}^{pi} is a tangent to the i -th parallel and \mathbf{T}^{mj} is a tangent to the j -th meridian. The tangential movement does not change the shape of a surface.

Let us have only one general curve Γ on the surface. This curve moves as the surface S moves. The parametrization $\Gamma = \{\mathbf{x}(u, t), u \in (0, 1), t \in (0, t_{end})\}$ determines a discretization of the curve. If we have n points on a curve Γ at time

Fig. 12 Illustration of the curve Γ on the surface S and $\mathbf{T}^\Gamma, \mathbf{N}_1^\Gamma, \mathbf{N}_2^\Gamma$



point m , points of the curve are $\mathbf{x}_i = \mathbf{x}(\frac{i}{n}, m)$. If the curve has a uniform distribution at time 0, we want to preserve this distribution. If it does not have the uniform distribution, we want redistribute points uniformly. Using this parametrization we can write $\mathbf{T}^\Gamma = \mathbf{x}_u / |\mathbf{x}_u|$.

There is another important parametrization of Γ . It is called the arc-length parametrization. We denote it by s . For this parametrization it holds $\frac{|d\mathbf{x}|}{ds} = 1$. Using this parametrization we can write $\mathbf{T}^\Gamma = \mathbf{x}_s$ and using the Frenet formula $k\mathbf{N}^\Gamma = \mathbf{T}_s^\Gamma = \mathbf{x}_{ss}$.

For better clarity, we have decided to denote the surface normal by \mathbf{N}^S and the surface mean curvature by k^S . Movement of the curve is split in three perpendicular directions: the direction \mathbf{T}^Γ which is a tangent vector of the curve Γ , and other two directions $\mathbf{N}_1^\Gamma, \mathbf{N}_2^\Gamma$ which lie in the normal plane of the curve Γ . The direction \mathbf{N}_1^Γ is chosen to be the normal vector of the surface \mathbf{N}^S . The third vector is $\mathbf{N}_2^\Gamma = \mathbf{N}_1^\Gamma \times \mathbf{T}^\Gamma$ (see the Fig. 12).

In general, the curve evolution is given by the equation

$$\partial_t \mathbf{x} = U^\Gamma \mathbf{N}_1^\Gamma + V^\Gamma \mathbf{N}_2^\Gamma + A^\Gamma \mathbf{T}^\Gamma, \quad (55)$$

where \mathbf{x} is the position vector of the curve Γ on the surface S . Since the curve is moving by (54), the values of U^Γ, V^Γ and A^Γ are given by

$$\begin{aligned} U^\Gamma &= \left(\varepsilon \left(k^S \mathbf{N}^S + f \mathbf{N}^S \right) \right) \cdot \mathbf{N}_1^\Gamma, \\ V^\Gamma &= \left(\varepsilon \left(k^S \mathbf{N}^S + f \mathbf{N}^S \right) \right) \cdot \mathbf{N}_2^\Gamma, \\ A^\Gamma &= \left(\varepsilon \left(k^S \mathbf{N}^S + f \mathbf{N}^S \right) \right) \cdot \mathbf{T}^\Gamma. \end{aligned} \quad (56)$$

Since $\mathbf{N}_1^\Gamma = \mathbf{N}^S$, $\mathbf{N}_2^\Gamma \perp \mathbf{N}^S$ and $\mathbf{T}^\Gamma \perp \mathbf{N}^S$ we have

$$\begin{aligned}
 U^\Gamma &= \varepsilon (k^S + f), \\
 V^\Gamma &= 0, \\
 A^\Gamma &= 0.
 \end{aligned} \tag{57}$$

Using these facts and by adding a new tangent velocity $\alpha^\Gamma \mathbf{T}^\Gamma$, we obtain

$$\partial_t \mathbf{x} = U^\Gamma \mathbf{N}_1^\Gamma + \alpha^\Gamma \mathbf{T}^\Gamma. \tag{58}$$

The scalar α^Γ is a quantity providing the tangential redistribution of points on the curve Γ . Since we do not want this velocity to move boundary points, we set $\alpha(0) = \alpha(1) = 0$.

Let us introduce a function $g^\Gamma = |\mathbf{x}_u| = \sqrt{\left(\frac{dx_1}{du}\right)^2 + \left(\frac{dx_2}{du}\right)^2 + \left(\frac{dx_3}{du}\right)^2} = \frac{ds}{du}$, which can be used for the point distribution. From the discrete point of view, g^Γ is proportional to a distance between points on the curve. Let us denote L^Γ the length of the curve Γ . If $\left(\frac{g^\Gamma}{L^\Gamma}\right)_t = 0$, the ratio of distances between points and length of the curve remains the same. This equation determines which α^Γ gives us an redistribution conserving initial one and it can be rewritten to

$$\left(\frac{g^\Gamma}{L^\Gamma}\right)_t = \frac{g^\Gamma}{L^\Gamma} (\alpha_s^\Gamma - U^\Gamma k_1^\Gamma + \langle U^\Gamma k_1^\Gamma \rangle_\Gamma). \tag{59}$$

The detailed process of obtaining Eq. (59) can be found in [44].

If we want to determinate g^Γ such that we obtain an asymptotically uniform redistribution, we can choose [47]

$$\left(\frac{g^\Gamma}{L^\Gamma}\right)_t = \omega \left(1 - \frac{g^\Gamma}{L^\Gamma}\right). \tag{60}$$

For change of $\left(\frac{g^\Gamma}{L^\Gamma}\right)_t$ in time holds Eq. (59) and after substituting it into Eq. (60), we can see that everything in (60) except the term α^Γ is given by the evolution of the curve and the surface. The equation (60) can be rewritten to

$$\alpha_s^\Gamma = -U^\Gamma k_1^\Gamma + \langle U^\Gamma k_1^\Gamma \rangle_\Gamma + \omega \left(\frac{L^\Gamma}{g^\Gamma} - 1\right), \tag{61}$$

from where we can determine α^Γ for any curve Γ on the surface S .

By adding such movement in direction of tangent vector of the curves, the final equation for the surface evolution, which includes also tangential evolution of points, is given by

$$\partial_t \mathbf{x} = \varepsilon (k\mathbf{N} + f\mathbf{N}) + \langle \alpha^\Gamma \mathbf{T}^\Gamma \rangle, \quad (62)$$

where $\langle \alpha^\Gamma \mathbf{T}^\Gamma \rangle = \sum_{\Gamma \in M^\Gamma} \alpha^\Gamma \mathbf{T}^\Gamma / |M^\Gamma|$ and M^Γ is the set of curves crossing in the point \mathbf{x} which we want to redistribute and $|M^\Gamma|$ is a cardinality of the set M^Γ . Since redistributions on crossing curves do not have to be compatible, we take the average value. In the continuous case, the Eqs. (62) and (54) give the same image of the evolving surface, but in the discrete case we obtain almost uniform point redistribution by using (62).

5.5 Numerical Approximation of Evolving Surface

Let us assume that the surface is composed by n_i meridians and n_j parallels. A point of an intersection of the i -th meridian and the j -th parallel in a time index t is denoted by \mathbf{x}_{ijt} . Let $p, q \in \{-1, 0, 1\}$ and let N_{int} denote a set of all (p, q) , $|p| + |q| = int$, where int denote an integer number. So points $\mathbf{x}_{i+p, j+q, t}$, $(p, q) \in N_1$ are north, south, east, west neighbouring points and points $\mathbf{x}_{i+p, j+q, t}$, $(p, q) \in N_2$ are north-east, north-west, south-east, south-west neighbouring points. If we do not specify that (p, q) belongs to N_1 or N_2 , we always consider that it belongs to the set N_1 .

The surface is divided into finite volumes. A finite volume V_{ijt} is associated with the point \mathbf{x}_{ijt} . Vertices of the finite volume are given by centers of line segments connecting points \mathbf{x}_{ijt} and $\mathbf{x}_{i+p, j+q, t}$, $(p, q) \in N_1$, and by centers of quadrilaterals given by points \mathbf{x}_{ijt} , $\mathbf{x}_{i+p, j, t}$, $\mathbf{x}_{i, j+q, t}$, $\mathbf{x}_{i+p, j+q, t}$, $(p, q) \in N_2$. These vertices are denoted by \mathbf{x}_{ijt}^{pq} , see Fig. 13, and they are computed by the formula

$$\mathbf{x}_{ijt}^{pq} = \frac{1}{4} \sum_{(l, m) \in B(p, q)} \mathbf{x}_{i+l, j+m, t}, \quad (63)$$

where $B(p, q) = \{(p, q), (p, 0), (0, q), (0, 0)\}$.

A boundary between V_{ijt} and $V_{i+p, j+q, t}$, $(p, q) \in N_1$ is kinked, so it is composed by two line segments. Let us denote by e_{ijt}^{pqr} , $(p, q) \in N_1$, $r \in \{-1, 1\}$, two line segments forming the boundary between the finite volumes V_{ijt} and $V_{i+p, j+q, t}$. Let us define a function, which generate a corner vertex of e_{ijt}^{pqr}

$$\odot(p, q, r) = \begin{cases} (r, q), & p = 0, \\ (p, r), & q = 0. \end{cases} \quad (64)$$

A line segment e_{ijt}^{pqr} is then given by points \mathbf{x}_{ijt}^{pq} and $\mathbf{x}_{i, j, t}^{\odot(p, q, r)}$. Let us denote \mathbf{n}_{ijt}^{pqr} an outer normal to the e_{ijt}^{pqr} . For better understanding see the Fig. 13.

Let k be equal to one for simplicity. By integrating (62) over the finite volume V_{ijt} we get

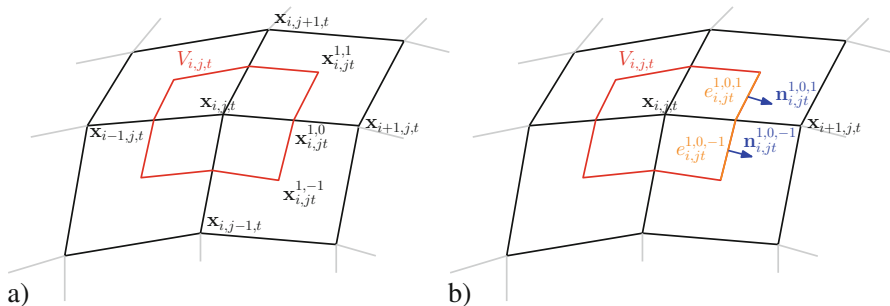


Fig. 13 The finite volume with representative points and finite volume with normals and edges

$$\int_{V_{ijt}} \partial_t \mathbf{x} dS = \int_{V_{ijt}} \Delta_s \mathbf{x} dS + \int_{V_{ijt}} f \mathbf{N} dS + \int_{V_{ijt}} \langle \alpha^\Gamma \mathbf{T}^\Gamma \rangle dS \quad (65)$$

and by using Green's theorem we have

$$\int_{V_{ijt}} \partial_t \mathbf{x} dS = \int_{\partial V_{ijt}} \nabla_s \mathbf{x} \cdot \mathbf{n}_{ijt} ds + \int_{V_{ijt}} f \mathbf{N} dS + \int_{V_{ijt}} \langle \alpha^\Gamma \mathbf{T}^\Gamma \rangle dS. \quad (66)$$

Using definition of the finite volume, the first term on the right-hand side of (66) can be rewritten as

$$\begin{aligned} \int_{\partial V_{ijt}} \nabla_s \mathbf{x} \cdot \mathbf{n}_{ijt} ds &= \sum_{(p,q) \in N_1} \sum_{r \in \{-1,1\}} \int_{e_{ijt}^{pqr}} \nabla_s \mathbf{x} \cdot \mathbf{n}_{ijt}^{pqr} ds = \\ &= \sum_{(p,q) \in N_1} \sum_{r \in \{-1,1\}} \int_{e_{ijt}^{pqr}} \frac{\partial \mathbf{x}}{\partial \mathbf{n}_{ijt}^{pqr}} ds. \end{aligned} \quad (67)$$

A derivative of \mathbf{x} in the direction of \mathbf{n}_{ijt}^{pqr} is considered constant on the boundary e_{ijt}^{pqr} . In general, a vector $\mathbf{x}_{i+p,j+q,t} - \mathbf{x}_{i,j,t}$ is not in the direction of the normal vector \mathbf{n}_{ijt}^{pqr} , so the derivative in the direction of the normal vector is approximated by a derivative in a direction of $\mathbf{x}_{i+p,j+q,t} - \mathbf{x}_{i,j,t}$ and a derivative in a direction of the tangent vector to e_{ijt}^{pqr} . The tangent vector to e_{ijt}^{pqr} is defined as

$$\mathbf{t}_{i,j,k}^{p,q,r} = \frac{\mathbf{x}_{i,j,k}^{\odot(p,q,r)} - \mathbf{x}_{i,j,k}^{pq}}{|\mathbf{x}_{i,j,k}^{\odot(p,q,r)} - \mathbf{x}_{i,j,k}^{pq}|}. \quad (68)$$

A unit vector \mathbf{v}_{ijt}^{pq} , which is pointing from the neighbouring point $\mathbf{x}_{i+p,j+q,t}$ to the point $\mathbf{x}_{i,j,t}$, is given by

$$\mathbf{v}_{ijt}^{pq} = \frac{\mathbf{x}_{i+p,j+q,t} - \mathbf{x}_{i,j,t}}{|\mathbf{x}_{i+p,j+q,t} - \mathbf{x}_{i,j,t}|}. \quad (69)$$

An approximation of the normal vector to e_{ijt}^{pqr} is defined as

$$\mathbf{n}_{ijt}^{pqr} = \frac{\mathbf{v}_{ijt}^{pq} \times \mathbf{t}_{i,j,k}^{p,q,r}}{|\mathbf{v}_{ijt}^{pq} \times \mathbf{t}_{i,j,k}^{p,q,r}|} \times \mathbf{t}_{i,j,k}^{p,q,r}. \quad (70)$$

Since vectors \mathbf{v}_{ijt}^{pq} , \mathbf{n}_{ijt}^{pqr} and \mathbf{t}_{ijt}^{pqr} lie in the same plane, the vector \mathbf{v}_{ijt}^{pq} can be expressed as a linear combination of \mathbf{n}_{ijt}^{pqr} and \mathbf{t}_{ijt}^{pqr} , and it holds

$$\nabla_s \mathbf{x} \cdot \mathbf{s}_{ijt}^{pqr} = \nabla_s \mathbf{x} \cdot (\beta_{ijt}^{pqr} \mathbf{n}_{ijt}^{pqr} + \gamma_{ijt}^{pqr} \mathbf{t}_{ijt}^{pqr}) = \beta_{ijt}^{pqr} \nabla_s \mathbf{x} \cdot \mathbf{n}_{ijt}^{pqr} + \gamma_{ijt}^{pqr} \nabla_s \mathbf{x} \cdot \mathbf{t}_{ijt}^{pqr} \quad (71)$$

where $\beta_{ijt}^{pqr} = \mathbf{n}_{ijt}^{pqr} \cdot \mathbf{v}_{ijt}^{pq}$ and $\gamma_{ijt}^{pqr} = \mathbf{t}_{ijt}^{pqr} \cdot \mathbf{v}_{ijt}^{pq}$. Thus the derivative in the normal direction can be expressed as

$$\nabla_s \mathbf{x} \cdot \mathbf{n}_{ijt}^{pqr} = \frac{1}{\beta_{ijt}^{pqr}} \nabla_s \mathbf{x} \cdot \mathbf{s}_{ijt}^{pqr} - \frac{\gamma_{ijt}^{pqr}}{\beta_{ijt}^{pqr}} \nabla_s \mathbf{x} \cdot \mathbf{t}_{ijt}^{pqr}, \quad (72)$$

and approximated by

$$\nabla_s \mathbf{x} \cdot \mathbf{n}_{ijt}^{pqr} = \frac{1}{\beta_{ijt}^{pqr}} \frac{\mathbf{x}_{i+p,j+q,t+1} - \mathbf{x}_{i,j,t+1}}{|\mathbf{x}_{i+p,j+q,t} - \mathbf{x}_{i,j,t}|} - \frac{\gamma_{ijt}^{pqr}}{\beta_{ijt}^{pqr}} \frac{\mathbf{x}_{i,j,t+1}^{\odot(p,q,r)} - \mathbf{x}_{i,j,t+1}^{pq}}{|\mathbf{x}_{i,j,t}^{\odot(p,q,r)} - \mathbf{x}_{i,j,t}^{pq}|}. \quad (73)$$

Using this equation and because the length of e_{ijt1}^{pqr} is equal to

$$m(e_{ijt1}^{pqr}) = |\mathbf{x}_{i,j,t}^{\odot(p,q,r)} - \mathbf{x}_{i,j,t}^{pq}|, \quad (74)$$

Eq. (67) can be approximated by

$$\sum_{(p,q) \in N_1} \sum_{r \in \{-1,1\}} \int_{e_{ijt}^{pqr}} \frac{\partial \mathbf{x}}{\partial \mathbf{n}_{ijt}^{pqr}} ds \approx \sum_{(p,q) \in N_1} \sum_{r \in \{-1,1\}} \left(\frac{m(e_{ijt1}^{pqr})}{\beta_{ijt}^{pqr}} \frac{\mathbf{x}_{i+p,j+q,t+1} - \mathbf{x}_{i,j,t+1}}{|\mathbf{x}_{i+p,j+q,t} - \mathbf{x}_{i,j,t}|} - \frac{\gamma_{ijt}^{pqr}}{\beta_{ijt}^{pqr}} \left(\mathbf{x}_{i,j,t+1}^{\odot(p,q,r)} - \mathbf{x}_{i,j,t+1}^{pq} \right) \right). \quad (75)$$

Because $\mathbf{x}_{i,j,t+1}^{\odot(p,q,r)}$ and $\mathbf{x}_{i,j,t+1}^{pq}$ are vertices of the finite volume computed as in (63), the equation can be rewritten

$$\sum_{(p,q) \in N_1} \sum_{r \in \{-1,1\}} \left(\frac{m(e_{ij,t}^{pqr})}{\beta_{ij,t}^{pqr}} \frac{\mathbf{x}_{i+p,j+q,t+1} - \mathbf{x}_{i,j,t+1}}{|\mathbf{x}_{i+p,j+q,t} - \mathbf{x}_{i,j,t}|} - \frac{\mathcal{V}_{ij,t}^{pqr}}{4\beta_{ij,t}^{pqr}} \left(\sum_{(l,m) \in B(\odot(p,q,r))} \mathbf{x}_{i+l,j+m,t+1} - \sum_{(l,m) \in B(p,q)} \mathbf{x}_{i+l,j+m,t+1} \right) \right). \quad (76)$$

A constant value of $f\mathbf{N}_{ij,t}$ is considered on the finite volume $V_{ij,t}$. So the second term on the right-hand side of the equation (66) can be rewritten as

$$\int_{V_{ij,t}} f\mathbf{N}dS = m(V_{ij,t})f\mathbf{N}_{ij,t}, \quad (77)$$

where $m(V_{ij,t})$ is a 2D measure of $V_{ij,t}$. In order to compute $\mathbf{N}_{ij,t}$, we consider a vector $k\mathbf{N}_{ij,t}$ computed by Eq. (76), where all values are taken at time index t . Then the normal vector to the surface is given by

$$\mathbf{N}_{ij,t} = \frac{k\mathbf{N}_{ij,t}}{|k\mathbf{N}_{ij,t}|}. \quad (78)$$

The meridians and parallels are curves according to which we are going to redistribute points on the surface. Only one meridian and one parallel go through the point $\mathbf{x}_{ij,t}$. Let us consider the i -th meridian and the j -th parallel. The point $\mathbf{x}_{ij,t}$ is the i -th point on the j -th parallel and the j -th point on the i -th parallel in time t . So we can write

$$\int_{V_{ij,t}} \langle \alpha^i \mathbf{T}^i \rangle dS = \int_{V_{ij,t}} \frac{\alpha^i \mathbf{T}^i + \alpha^j \mathbf{T}^j}{2} dS, \quad (79)$$

where \mathbf{T}^i (\mathbf{T}^j) is the tangent vector to the i -th meridian (j -th parallel). Values of $\alpha^i \mathbf{T}^i$ and $\alpha^j \mathbf{T}^j$ are considered constant on $V_{ij,t}$ and we approximate them using central differences

$$\begin{aligned} & \int_{V_{ij,t}} \frac{\alpha^i \mathbf{T}^i + \alpha^j \mathbf{T}^j}{2} dS = \\ & = \frac{m(V_{ij,t})}{2} \cdot \left(\alpha_{j,t}^i \frac{\mathbf{x}_{i,j+1,t+1} - \mathbf{x}_{i,j-1,t+1}}{|\mathbf{x}_{i,j+1,t} - \mathbf{x}_{i,j-1,t}|} + \alpha_{i,t}^j \frac{\mathbf{x}_{i+1,j,t+1} - \mathbf{x}_{i-1,j,t+1}}{|\mathbf{x}_{i,j+1,t} - \mathbf{x}_{i,j-1,t}|} \right) \end{aligned} \quad (80)$$

where α_{jt}^i (α_{it}^j) is α^i (α^j) in the j -th (i -th) point on the i -th (j -th) parallel in time t . A time derivative is considered constant on the finite volume and is approximated by a finite difference

$$\int_{V_{ijt}} \partial_t \mathbf{x} dS = m(V_{ijt}) \left(\frac{\mathbf{x}_{i,j,t+1} - \mathbf{x}_{ijt}}{\Delta t} \right). \quad (81)$$

Using Eqs. (75), (77), (80), and (81), we get

$$\begin{aligned} m(V_{ijt}) \left(\frac{\mathbf{x}_{i,j,t+1} - \mathbf{x}_{ijt}}{\Delta t} \right) &= \sum_{(p,q) \in N_1} \sum_{r \in \{-1,1\}} \left(\frac{m(e_{ijt}^{pqr})}{\beta_{ijt}^{pqr}} \frac{\mathbf{x}_{i+p,j+q,t+1} - \mathbf{x}_{i,j,t+1}}{|\mathbf{x}_{i+p,j+q,t} - \mathbf{x}_{i,j,t}|} \right. \\ &\quad \left. - \frac{\alpha_{ijt}^{pqr}}{4\beta_{ijt}^{pqr}} \left(\sum_{(l,m) \in B(\odot(p,q,r))} \mathbf{x}_{i+l,j+m,t+1} - \sum_{(l,m) \in B(p,q)} \mathbf{x}_{i+l,j+m,t+1} \right) \right) \\ &\quad + m(V_{ijt}) f \mathbf{N}_{ijt} \\ &\quad + \frac{m(V_{ijt})}{2} \left(\alpha_{jt}^i \frac{\mathbf{x}_{i,j+1,t+1} - \mathbf{x}_{i,j-1,t+1}}{|\mathbf{x}_{i,j+1,t} - \mathbf{x}_{i,j-1,t}|} + \alpha_{it}^j \frac{\mathbf{x}_{i+1,j,t+1} - \mathbf{x}_{i-1,j,t+1}}{|\mathbf{x}_{i+1,j,t} - \mathbf{x}_{i-1,j,t}|} \right). \end{aligned} \quad (82)$$

We have a system of $n_i \times n_j$ equations with $n_i \times n_j$ unknowns $\mathbf{x}_{ij,t+1}$, where $i = 1, \dots, n_i$ and $j = 1, \dots, n_j$.

Values of α_{jt}^i (α_{it}^j respectively) are computed before the system of equations (82) is solved. We obtain these values by solving Eq. (61). Approximating the derivative in (61) by using the backward difference and taking the right-hand side in the discrete points we get

$$\frac{\alpha_{jt}^i - \alpha_{j-1,t}^i}{|\mathbf{x}_{i,j,t} - \mathbf{x}_{i,j-1,t}|} = U_{j-1/2,t}^i k_{1,j-1/2,t}^i - \langle U_t^i k_{1t}^i \rangle_i + \omega \left(\frac{L_t^i |\mathbf{x}_{i,j,t} - \mathbf{x}_{i,j-1,t}|}{n_j} - 1 \right) \quad (83)$$

where

$$k_{m,j-1/2,t}^i = \left(k_{m,jt}^i - k_{m,j-1,t}^i \right) / 2, \quad m = 1, 2 \quad (84)$$

$$k_{m,jt}^i = k \mathbf{N}_{jt}^i \cdot \mathbf{N}_{m,jt}^i, \quad m = 1, 2 \quad (85)$$

$$\mathbf{N}_{1,jt}^i = \mathbf{N}_{jt}^i, \quad (86)$$

$$\mathbf{N}_{2,jt}^i = \mathbf{N}_{1,jt}^i \times \mathbf{T}_{jt}^i, \quad (87)$$

$$\mathbf{T}_{jt}^i = \frac{\mathbf{x}_{i,j+1,t} - \mathbf{x}_{i,j-1,t}}{|\mathbf{x}_{i,j+1,t} - \mathbf{x}_{i,j-1,t}|}, \quad (88)$$

$$k\mathbf{N}_{jt}^i = \frac{\frac{\mathbf{x}_{i,j+1,t} - \mathbf{x}_{i,j,t}}{|\mathbf{x}_{i,j+1,t} - \mathbf{x}_{i,j,t}|} - \frac{\mathbf{x}_{i,j,t} - \mathbf{x}_{i,j-1,t}}{|\mathbf{x}_{i,j,t} - \mathbf{x}_{i,j-1,t}|}}{(|\mathbf{x}_{i,j+1,t} - \mathbf{x}_{i,j,t}| + |\mathbf{x}_{i,j,t} - \mathbf{x}_{i,j-1,t}|)/2}, \quad (89)$$

$$U_{j-1/2,t}^i = \left(U_{j+1,t}^i + U_{j,t}^i \right) / 2, \quad (90)$$

$$U_{j,t}^i = (\varepsilon k \mathbf{N}_{ijt} + f \mathbf{N}_{ijt}) \cdot \mathbf{N}_{1,jt}^i, \quad (91)$$

$$\langle U^i k_1^i \rangle_i = \frac{1}{L_t^i} \sum_{l=1}^{n_j} h_{il} (U_{l-1/2}^i k_{1,l-1/2}^i), \quad (92)$$

$$L_t^i = \sum_{i=1}^{n_j} |\mathbf{x}_{i,jt} - \mathbf{x}_{i,j-1,t}|. \quad (93)$$

From (83), (93) and (93) we get

$$\begin{aligned} \alpha_{jt}^i &= \alpha_{j-1,t}^i - |\mathbf{x}_{i,jt} - \mathbf{x}_{i,j-1,t}| \left(U_{j-1/2,t}^i k_{1,j-1/2,t}^i \right) + \\ &+ |\mathbf{x}_{i,jt} - \mathbf{x}_{i,j-1,t}| \sum_{l=1}^{n_j} |\mathbf{x}_{i,lt} - \mathbf{x}_{i,l-1,t}| \left(U_{l-1/2,t}^i k_{1,l-1/2,t}^i \right) + \\ &+ \omega \left(\frac{L_t^i}{n_j} - |\mathbf{x}_{i,jt} - \mathbf{x}_{i,j-1,t}| \right). \end{aligned} \quad (94)$$

Because $\alpha_{0,t}^i = 0$ ($\alpha_{0,t}^j = 0$), every value of α_{jt}^i (α_{jt}^j) can be computed before solving system of equations (81). The system of equations (82) can be solved using the BiCGSTAB method [4, 54].

5.6 Discretization of the Oblique Derivative BVP for the Laplace Equation

5.6.1 Approximation of the Laplace Equation

In this section, we introduce FVM for a discretization of Eq. (4) on a non-uniform grids.

We discretize the domain Ω by the non-uniform regular hexahedron grid using the approach described in the previous section. Such constructed vertices are representative points of finite volumes. Vertices of the finite volume $\mathbf{x}_{i,j,k}^{p,q,r}$ are constructed in the center of eight neighbouring representative points using Eq. (36),

Using the same principles as in Eqs. (30) and (31) we obtain Eq. (32). Unlike for uniform grids, where the vector $\mathbf{x}_{j+p,j+q,k+r} - \mathbf{x}_{i,j,k}$ and the normal vector $\mathbf{n}_{i,j,k}^{p,q,r}$ are parallel, we can not use Eq. (33) to approximate the normal derivative. For this approximation we utilize the same idea as in Sect. 5.1 of splitting a derivative in the directions of three linearly independent directions.

One of the vectors is the unit vector $\mathbf{v}_{i,j,k}^{p,q,r}$, which is pointing from the neighbouring point $\mathbf{x}_{i,j,k}$ to the point $\mathbf{x}_{i+p,j+q,k+r}$, and is given by

$$\mathbf{v}_{i,j,k}^{p,q,r} = \frac{\mathbf{x}_{i+p,j+q,k+r} - \mathbf{x}_{i,j,k}}{|\mathbf{x}_{i+p,j+q,k+r} - \mathbf{x}_{i,j,k}|}. \quad (95)$$

Let us introduce new operations on the set N_1

$$\begin{aligned} \oplus(p, q, r) &= \begin{cases} (p, 1, 1), & p \neq 0 \\ (1, q, 1), & q \neq 0 \\ (1, 1, r), & r \neq 0 \end{cases} \\ \ominus(p, q, r) &= \begin{cases} (p, -1, -1), & p \neq 0 \\ (-1, q, -1), & q \neq 0 \\ (-1, -1, r), & r \neq 0 \end{cases} \\ \boxplus(p, q, r) &= \begin{cases} (p, 1, -1), & p \neq 0 \\ (1, q, -1), & q \neq 0 \\ (1, -1, r), & r \neq 0 \end{cases} \\ \boxminus(p, q, r) &= \begin{cases} (p, -1, 1), & p \neq 0 \\ (-1, q, 1), & q \neq 0 \\ (-1, 1, r), & r \neq 0 \end{cases} \end{aligned}$$

Thanks to these operations we can write the vertices of the boundary $e_{i,j,k}^{p,q,r}$ as $\mathbf{x}_{i,j,k}^{\boxplus(p,q,r)}$, $\mathbf{x}_{i,j,k}^{\boxminus(p,q,r)}$, $\mathbf{x}_{i,j,k}^{\oplus(p,q,r)}$ and $\mathbf{x}_{i,j,k}^{\ominus(p,q,r)}$. These vertices are used to compute tangent vectors. The first tangent vector $\mathbf{t}_{i,j,k}^{p,q,r}$ to the boundary between $e_{i,j,k}^{p,q,r}$ is given by

$$\mathbf{t}_{i,j,k}^{p,q,r} = \frac{\mathbf{x}_{i,j,k}^{\oplus(p,q,r)} - \mathbf{x}_{i,j,k}^{\ominus(p,q,r)}}{|\mathbf{x}_{i,j,k}^{\oplus(p,q,r)} - \mathbf{x}_{i,j,k}^{\ominus(p,q,r)}|}. \quad (96)$$

The second tangent vector $\mathbf{f}_{i,j,k}^{p,q,r}$ is given by other two vertices of $e_{i,j,k}^{p,q,r}$,

$$\mathbf{f}_{i,j,k}^{p,q,r} = \frac{\mathbf{x}_{i,j,k}^{\boxplus(p,q,r)} - \mathbf{x}_{i,j,k}^{\boxminus(p,q,r)}}{|\mathbf{x}_{i,j,k}^{\boxplus(p,q,r)} - \mathbf{x}_{i,j,k}^{\boxminus(p,q,r)}|}. \quad (97)$$

The normal vector to the boundary of the finite volume is then defined by

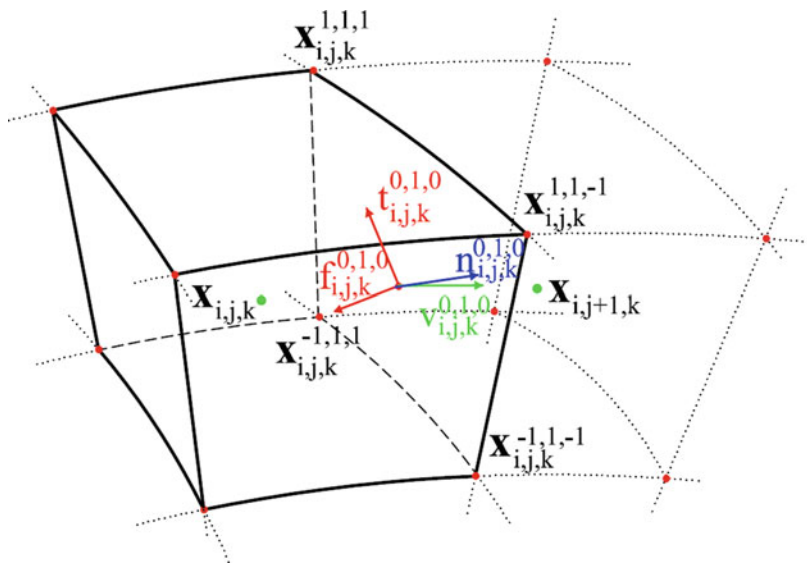


Fig. 14 The finite volume

$$\mathbf{n}_{i,j,k}^{p,q,r} = \mathbf{t}_{i,j,k}^{p,q,r} \times \mathbf{f}_{i,j,k}^{p,q,r}. \quad (98)$$

where $\mathbf{n}_{i,j,k}^{p,q,r}$ is the outer normal relative to the finite volume $V_{i,j,k}$ (see Fig. 14).

Since the vector $\mathbf{v}_{i,j,k}^{pqr}$ can be expressed as a linear reconstruction of $\mathbf{n}_{i,j,k}^{pqr}$, $\mathbf{t}_{i,j,k}^{pqr}$ and $\mathbf{f}_{i,j,k}^{pqr}$, it holds

$$\begin{aligned} \nabla T \cdot \mathbf{v}_{i,j,k}^{pqr} &= \nabla T \cdot (\beta_{i,j,k}^{pqr} \mathbf{n}_{i,j,k}^{pqr} + \alpha_{i,j,k}^{pqr} \mathbf{t}_{i,j,k}^{pqr} + \gamma_{i,j,k}^{pqr} \mathbf{f}_{i,j,k}^{pqr}) \\ &= \beta_{i,j,k}^{pqr} \nabla T \cdot \mathbf{n}_{i,j,k}^{pqr} + \alpha_{i,j,k}^{pqr} \nabla T \cdot \mathbf{t}_{i,j,k}^{pqr} + \gamma_{i,j,k}^{pqr} \nabla T \cdot \mathbf{f}_{i,j,k}^{pqr}, \end{aligned} \quad (99)$$

where coefficients $\alpha_{i,j,k}^{pqr}$, $\beta_{i,j,k}^{pqr}$ and $\gamma_{i,j,k}^{pqr}$ are given by solving a linear system of equations

$$\mathbf{v}_{i,j,k}^{pqr} = \beta_{i,j,k}^{pqr} \mathbf{n}_{i,j,k}^{pqr} + \alpha_{i,j,k}^{pqr} \mathbf{t}_{i,j,k}^{pqr} + \gamma_{i,j,k}^{pqr} \mathbf{f}_{i,j,k}^{pqr}. \quad (100)$$

Therefore, for the derivative in the direction of normal we get

$$\nabla T \cdot \mathbf{n}_{i,j,k}^{pqr} = \frac{1}{\beta_{i,j,k}^{pqr}} (\nabla T \cdot \mathbf{v}_{i,j,k}^{pqr} - \alpha_{i,j,k}^{pqr} \nabla T \cdot \mathbf{t}_{i,j,k}^{pqr} - \gamma_{i,j,k}^{pqr} \nabla T \cdot \mathbf{f}_{i,j,k}^{pqr}). \quad (101)$$

Equation (101) is approximated by

$$\begin{aligned} \frac{1}{\beta_{ijk}^{pqr}} (\nabla T \cdot \mathbf{v}_{ijk}^{pqr} - \alpha_{ijk}^{pqr} \nabla T \cdot \mathbf{t}_{ijk}^{pqr} - \gamma_{ijk}^{pqr} \nabla T \cdot \mathbf{f}_{ijk}^{pqr}) \approx \\ \frac{1}{\beta_{ijk}^{pqr}} \frac{T_{ijk} - T_{i+p,j+q,k+r}}{d_{ijk}^{pqr}} - \frac{\alpha_{ijk}^{pqr}}{\beta_{ijk}^{pqr}} \frac{T_{i,j,k}^{\oplus(p,q,r)} - T_{i,j,k}^{\ominus(p,q,r)}}{|\mathbf{x}_{i,j,k}^{\oplus(p,q,r)} - \mathbf{x}_{i,j,k}^{\ominus(p,q,r)}|} \\ - \frac{\gamma_{ijk}^{pqr}}{\beta_{ijk}^{pqr}} \frac{T_{i,j,k}^{\boxplus(p,q,r)} - T_{i,j,k}^{\boxminus(p,q,r)}}{|\mathbf{x}_{i,j,k}^{\boxplus(p,q,r)} - \mathbf{x}_{i,j,k}^{\boxminus(p,q,r)}|}, \end{aligned} \quad (102)$$

where $T_{i,j,k}^{\oplus(p,q,r)}$ are the values at the points $\mathbf{x}_{i,j,k}^{\oplus(p,q,r)}$.

Equation (32) can be rewritten using Eq. (102) in the form

$$\begin{aligned} - \sum_{(p,q,r) \in N_1} m(e_{ijk}^{pqr}) \left(\frac{1}{\beta_{ijk}^{pqr}} \frac{T_{ijk} - T_{i+p,j+q,k+r}}{d_{ijk}^{pqr}} \right. \\ \left. - \frac{\alpha_{ijk}^{pqr}}{\beta_{ijk}^{pqr}} \frac{T_{i,j,k}^{\oplus(p,q,r)} - T_{i,j,k}^{\ominus(p,q,r)}}{|\mathbf{x}_{i,j,k}^{\oplus(p,q,r)} - \mathbf{x}_{i,j,k}^{\ominus(p,q,r)}|} - \frac{\gamma_{ijk}^{pqr}}{\beta_{ijk}^{pqr}} \frac{T_{i,j,k}^{\boxplus(p,q,r)} - T_{i,j,k}^{\boxminus(p,q,r)}}{|\mathbf{x}_{i,j,k}^{\boxplus(p,q,r)} - \mathbf{x}_{i,j,k}^{\boxminus(p,q,r)}|} \right) = 0. \end{aligned} \quad (103)$$

For the finite volumes, that are adjacent to the boundary finite volumes, the value $T_{i+p,j+q,k+r}$ is given by the Dirichlet BC (6). Similarly as in Eq. 42 the values $T_{i,j,k}^{\oplus(p,q,r)}$ are not given in representative points, but in points $\mathbf{x}_{i,j,k}^{\oplus(p,q,r)}$, which are vertices of the finite volume. They are at the center of the corresponding representative points (36). So values $T_{i,j,k}^{\oplus(p,q,r)}$ are approximated by

$$T_{i,j,k}^{\oplus(p,q,r)} = T(\mathbf{x}_{i,j,k}^{\oplus(p,q,r)}) = \frac{1}{8} \sum_{(l,m,n) \in B(\oplus(p,q,r))} T_{i+l,j+m,k+n}, \quad (104)$$

and values $T_{i,j,k}^{\ominus(p,q,r)}$, $T_{i,j,k}^{\boxplus(p,q,r)}$, $T_{i,j,k}^{\boxminus(p,q,r)}$ in Eq. (103) can be expressed similarly.

It is worth noting that for an uniform grid Eq. (103) is the same as Eq. (35).

5.6.2 Approximation of the Oblique Derivative Boundary Condition

In this section we introduce a higher order discretization of the oblique derivative BC (5).

The computational domain is divided by finite volumes as in the previous subsection. However, the finite volumes are constructed also around representative points on the boundary Γ . Vertices common to boundary finite volumes and inner finite volumes are located at the center of the representative points defined by (36). Other vertices of the boundary finite volumes are obtained by mirroring of the former ones through Γ . The set of added finite volumes is denoted by O .

As in Sect. 5.1, we understand Eq. (5) as an advection equation and we can obtain Eq. (50) using the same principles.

The difference between this method and the first order upwind method is in the approximation of the value $T_{i,j,k}^{p,q,r}$. In this case, we do not simply assign a value $T_{i,j,k}$ or $T_{i+p,j+q,k+r}$ to the boundary but we correct it using a gradient. Using this method there are two ways how to approximate the value $T_{i,j,k}^{p,q,r}$

$$T_{i,j,k}^{p,q,r} = T_{i,j,k} + \nabla T_{i,j,k} \cdot (\mathbf{x}_{i,j,k}^{p,q,r} - \mathbf{x}_{i,j,k}), \quad (105)$$

$$T_{i,j,k}^{p,q,r} = T_{i+p,j+q,k+r} + \nabla T_{i+p,j+q,k+r} \cdot (\mathbf{x}_{i,j,k}^{p,q,r} - \mathbf{x}_{i+p,j+q,k+r}), \quad (106)$$

We choose an appropriate approximation using an upwind method. If $s_{i,j,k}^{p,q,r} > 0$ we use Eqs. (105) and (106) otherwise. Then Eq. (50) becomes

$$\begin{aligned} & \sum_{(p,q,r) \in N_1^{in}(i,j,k)} (T_{i+p,j+q,k+r} + \nabla T_{i+p,j+q,k+r} \cdot (\mathbf{x}_{i,j,k}^{p,q,r} - \mathbf{x}_{i+p,j+q,k+r})) s_{i,j,k}^{p,q,r} \\ & + \sum_{(p,q,r) \in N_1^{out}(i,j,k)} (T_{i,j,k} + \nabla T_{i,j,k} \cdot (\mathbf{x}_{i,j,k}^{p,q,r} - \mathbf{x}_{i,j,k})) s_{i,j,k}^{p,q,r} \\ & - \sum_{(p,q,r) \in N_1^{in}(i,j,k)} T_{i,j,k} s_{i,j,k}^{p,q,r} - \sum_{(p,q,r) \in N_1^{out}(i,j,k)} T_{i,j,k} s_{i,j,k}^{p,q,r} = |V_{i,j,k}| \delta g. \end{aligned} \quad (107)$$

By using the functions $\max(0, s_{i,j,k}^{p,q,r})$ and $\min(0, s_{i,j,k}^{p,q,r})$ we can write

$$\begin{aligned} & \sum_{(p,q,r) \in N_1} \left[(T_{i+p,j+q,k+r} + \nabla T_{i+p,j+q,k+r} \cdot (\mathbf{x}_{i,j,k}^{p,q,r} - \mathbf{x}_{i+p,j+q,k+r})) \min(0, s_{i,j,k}^{p,q,r}) \right. \\ & \left. + (T_{i,j,k} + \nabla T_{i,j,k} \cdot (\mathbf{x}_{i,j,k}^{p,q,r} - \mathbf{x}_{i,j,k})) \max(0, s_{i,j,k}^{p,q,r}) - T_{i,j,k} s_{i,j,k}^{p,q,r} \right] = |V_{i,j,k}| \delta g. \end{aligned} \quad (108)$$

The gradient on the finite volume $V_{i,j,k}$ can be expressed using derivatives in three linear independent directions. Let us denote these directions \mathbf{p} , \mathbf{q} , \mathbf{r} . For derivatives in these directions applies

$$\begin{aligned} \frac{\partial T}{\partial \mathbf{p}} &= \nabla T \cdot \mathbf{p} = \frac{\partial T}{\partial x} p_x + \frac{\partial T}{\partial y} p_y + \frac{\partial T}{\partial z} p_z, \\ \frac{\partial T}{\partial \mathbf{q}} &= \nabla T \cdot \mathbf{q} = \frac{\partial T}{\partial x} q_x + \frac{\partial T}{\partial y} q_y + \frac{\partial T}{\partial z} q_z, \\ \frac{\partial T}{\partial \mathbf{r}} &= \nabla T \cdot \mathbf{r} = \frac{\partial T}{\partial x} r_x + \frac{\partial T}{\partial y} r_y + \frac{\partial T}{\partial z} r_z. \end{aligned} \quad (109)$$

If we look at (109) as a system of linear equations for unknowns $\frac{\partial T}{\partial x}$, $\frac{\partial T}{\partial y}$, $\frac{\partial T}{\partial z}$, we obtain the solution

$$\begin{aligned}\frac{\partial T}{\partial x} &= -\frac{-p_z q_y \frac{\partial T}{\partial \mathbf{r}} + p_y q_z \frac{\partial T}{\partial \mathbf{r}} - q_z \frac{\partial T}{\partial \mathbf{p}} r_y + p_z \frac{\partial T}{\partial \mathbf{q}} r_y + q_y \frac{\partial T}{\partial \mathbf{p}} r_z - p_y \frac{\partial T}{\partial \mathbf{q}} r_z}{p_z q_y r_x - p_y q_z r_x - p_z q_x r_y + p_x q_z r_y + p_y q_x r_z - p_x q_y r_z}, \\ \frac{\partial T}{\partial y} &= -\frac{p_z q_x \frac{\partial T}{\partial \mathbf{r}} - p_x q_z \frac{\partial T}{\partial \mathbf{r}} + q_z \frac{\partial T}{\partial \mathbf{p}} r_x - p_z \frac{\partial T}{\partial \mathbf{q}} r_x - q_x \frac{\partial T}{\partial \mathbf{p}} r_z + p_x \frac{\partial T}{\partial \mathbf{q}} r_z}{p_z q_y r_x - p_y q_z r_x - p_z q_x r_y + p_x q_z r_y + p_y q_x r_z - p_x q_y r_z}, \\ \frac{\partial T}{\partial z} &= -\frac{-p_y q_x \frac{\partial T}{\partial \mathbf{r}} + p_x q_y \frac{\partial T}{\partial \mathbf{r}} - q_y \frac{\partial T}{\partial \mathbf{p}} r_x + p_y \frac{\partial T}{\partial \mathbf{q}} r_x + q_x \frac{\partial T}{\partial \mathbf{p}} r_y - p_x \frac{\partial T}{\partial \mathbf{q}} r_y}{p_z q_y r_x - p_y q_z r_x - p_z q_x r_y + p_x q_z r_y + p_y q_x r_z - p_x q_y r_z},\end{aligned}\quad (110)$$

and thus

$$\nabla T_{i,j,k} = \frac{\mathbf{p} \times \mathbf{q} \frac{\partial T}{\partial \mathbf{r}} + \mathbf{q} \times \mathbf{r} \frac{\partial T}{\partial \mathbf{p}} + \mathbf{r} \times \mathbf{p} \frac{\partial T}{\partial \mathbf{q}}}{\det(\mathbf{p}, \mathbf{q}, \mathbf{r})}, \quad (111)$$

where

$$\det(\mathbf{p}, \mathbf{q}, \mathbf{r}) = \det \begin{pmatrix} p_x & p_y & p_z \\ q_x & q_y & q_z \\ r_x & r_y & r_z \end{pmatrix}. \quad (112)$$

If the finite volume, on which we want to reconstruct the gradient, is the inner finite volume, then \mathbf{p} , \mathbf{q} , \mathbf{r} are defined by

$$\begin{aligned}\mathbf{p} &= \frac{\mathbf{x}_{i+1,j,k} - \mathbf{x}_{i-1,j,k}}{|\mathbf{x}_{i+1,j,k} - \mathbf{x}_{i-1,j,k}|}, \\ \mathbf{q} &= \frac{\mathbf{x}_{i,j+1,k} - \mathbf{x}_{i,j-1,k}}{|\mathbf{x}_{i,j+1,k} - \mathbf{x}_{i,j-1,k}|}, \\ \mathbf{r} &= \frac{\mathbf{x}_{i,j,k+1} - \mathbf{x}_{i,j,k-1}}{|\mathbf{x}_{i,j,k+1} - \mathbf{x}_{i,j,k-1}|}.\end{aligned}\quad (113)$$

Approximation of derivatives in these directions are

$$\begin{aligned}\frac{\partial T}{\partial \mathbf{p}} &\approx \frac{T_{i+1,j,k} - T_{i-1,j,k}}{|\mathbf{x}_{i+1,j,k} - \mathbf{x}_{i-1,j,k}|}, \\ \frac{\partial T}{\partial \mathbf{q}} &\approx \frac{T_{i,j+1,k} - T_{i,j-1,k}}{|\mathbf{x}_{i,j+1,k} - \mathbf{x}_{i,j-1,k}|}, \\ \frac{\partial T}{\partial \mathbf{r}} &\approx \frac{T_{i,j,k+1} - T_{i,j,k-1}}{|\mathbf{x}_{i,j,k+1} - \mathbf{x}_{i,j,k-1}|}.\end{aligned}\quad (114)$$

On the other hand, if the finite volume is the boundary finite volume then one of the neighbouring finite volumes does not exist. Let say the finite volume $V_{i-1,j,k}$ does not exist. Then we cannot use $T_{i-1,j,k}$ for reconstruction but we can use the oblique derivative $g(\mathbf{x}_{ijk})$ in direction $\mathbf{s}(\mathbf{x}_{ijk})$. Let us denote them g and \mathbf{s} . Then \mathbf{p} , \mathbf{q} , \mathbf{r} are defined by

$$\begin{aligned}\mathbf{p} &= \mathbf{s}, \\ \mathbf{q} &= \frac{\mathbf{x}_{i,j+1,k} - \mathbf{x}_{i,j-1,k}}{|\mathbf{x}_{i,j+1,k} - \mathbf{x}_{i,j-1,k}|}, \\ \mathbf{r} &= \frac{\mathbf{x}_{i,j,k+1} - \mathbf{x}_{i,j,k-1}}{|\mathbf{x}_{i,j,k+1} - \mathbf{x}_{i,j,k-1}|}.\end{aligned}\quad (115)$$

Approximation of derivatives in these directions are

$$\begin{aligned}\frac{\partial T}{\partial \mathbf{p}} &= \delta g, \\ \frac{\partial T}{\partial \mathbf{q}} &\approx \frac{T_{i,j+1,k} - T_{i,j-1,k}}{|\mathbf{x}_{i,j+1,k} - \mathbf{x}_{i,j-1,k}|}, \\ \frac{\partial T}{\partial \mathbf{r}} &\approx \frac{T_{i,j,k+1} - T_{i,j,k-1}}{|\mathbf{x}_{i,j,k+1} - \mathbf{x}_{i,j,k-1}|},\end{aligned}\quad (116)$$

and so

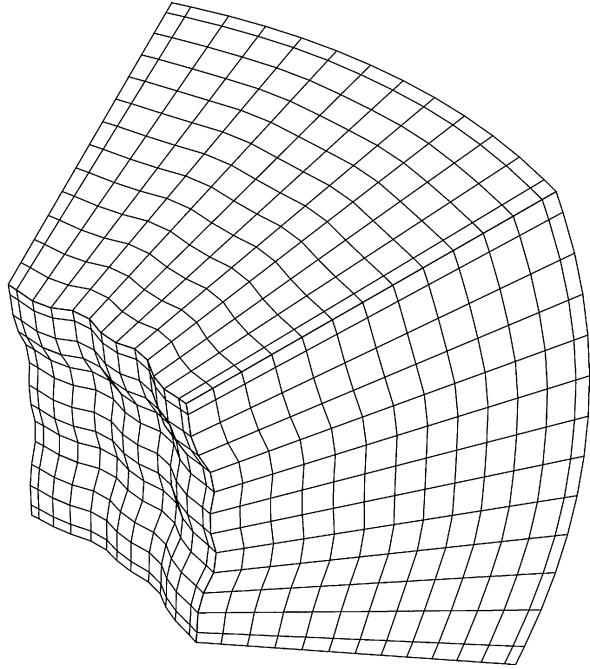
$$\nabla T_{i,j,k} = \frac{\mathbf{s} \times \mathbf{q} \frac{T_{i,j,k+1} - T_{i,j,k-1}}{|\mathbf{x}_{i,j,k+1} - \mathbf{x}_{i,j,k-1}|} + \mathbf{q} \times \mathbf{r} \delta g + \mathbf{r} \times \mathbf{s} \frac{T_{i,j+1,k} - T_{i,j-1,k}}{|\mathbf{x}_{i,j+1,k} - \mathbf{x}_{i,j-1,k}|}}{\det(\mathbf{s}, \mathbf{q}, \mathbf{r})}.\quad (117)$$

Substituting Eq. (117) into Eq. (108), we get equations for boundary finite volumes $V_{i,j,k} \in O$. Due to the construction of our scheme, the equations for these finite volumes may require two neighbouring finite volumes in the directions of \mathbf{q} and \mathbf{r} . For those which do not have such neighbours, we have to prescribe Dirichlet BC, which is also in accordance with the compatibility of BCs mentioned in the introduction. All these equations, together with equations from the discretization of the Laplace equation form a numerical scheme for solving the BVP (4), (5) and (6).

5.7 Numerical Experiments

In the first experiment we solve the BVP (4), (5) and (6) with BCs obtained from an artificial harmonic function defined on a computational domain, see Fig. 15. This computational domain is bounded by four planar side boundaries, a spherical upper boundary and by the bottom boundary given by a perturbed sphere. In order to test

Fig. 15 Computational domain for the first experiment



the numerical scheme, we constructed the most coarse grid. Then refined grids were constructed by adding new representative points in-between representative points of the previous grid using Eq. (36). The exact solution was chosen as $T(\mathbf{x}) = \frac{1}{|\mathbf{x} - (0.1, 0.2, 0.3)|}$ and its values were used to generate the oblique derivative and the Dirichlet BC. The oblique derivative BC were prescribed on the perturbed sphere as the bottom boundary. The vectors in the direction of $\nabla T(\mathbf{x})$ were rotated alternately by the angle of $\pi/6$ around x , y , z axes to get the vectors v , see Fig. 16. Table 7 depicts the L_2 -norm and maximum norm of residuals between the obtained FVM solutions and the exact solution and the achieved EOC.

The second experiment is computed on the same computational domain with the exact solution taken from EGM2008 while using only the SH coefficients up to degree and order 5. The oblique derivative is generated as the first derivative of the disturbing potential (the exact solution) in the radial direction. This radial direction represents the oblique direction since it differs from the direction of the normal vector to the bottom boundary. Table 8 shows the L_2 -norm and maximum norm of residuals between the obtained FVM solutions and exact solution, and the achieved EOC. Both experiments show that EOC of our FVM approach is about 1.6, which means that if we decrease the maximal size of the finite volumes by 2 then the error of our solution will decrease approximately by 3 ($2^{1.6} \approx 3.03$).

Following numerical experiments were performed in the domain above the Himalayas bounded by $\langle 60^\circ, 110^\circ \rangle$ meridians and $\langle 20^\circ, 50^\circ \rangle$ parallels. The EGM2008 up to degree 2160 was used to generate all BCs and the harmonic function. The

Fig. 16 Oblique derivative directions for the first experiment

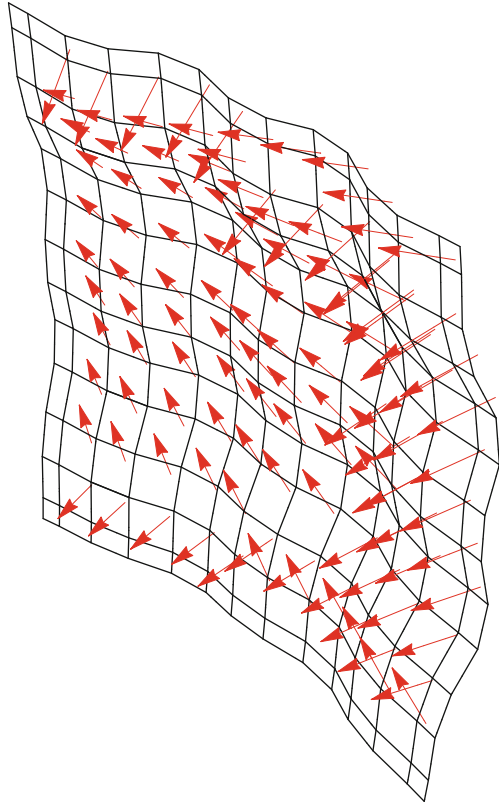


Table 7 The L_2 norm and max norm of residuals, and EOC of FVM for the problem with the exact solution $T(\mathbf{x}) = |\mathbf{x} - (0.1, 0.2, 0.3)|^{-1}$

h_{\max}	$\ e_{h_{\max}}\ _{L_2}$	EOC	$\ e_{h_{\max}}\ _{\max}$	EOC $_{\max}$
0.125	0.000229	–	0.00269	–
0.0642	7.00358e–05	1.761	0.00102	1.429
0.0324	2.43723e–05	1.545	0.000418	1.31582
0.0162	7.90755e–06	1.635	0.000153	1.45607
0.00817	2.44251e–06	1.702	5.23081e–05	1.56279

bottom boundary was given by grid points that are located on the Earth’s surface. Their spacing in horizontal directions was uniform. Their heights were interpolated from the SRTM30 PLUS topography model [6], see Fig. 17a. An upper boundary was chosen in the height of 240 km above a reference ellipsoid corresponding to an average altitude of the GOCE satellite orbits. The resulting 3D computational grid constructed by our surface evolution method is non-uniform. On the bottom boundary the first derivatives in the radial direction were prescribed that represented the oblique derivative BC. On the rest of the boundary the Dirichlet BC in form of the disturbing potential were prescribed. All these BCs were generated from the EGM2008 model up to degree 2160.

Table 8 The L_2 norm and max norm of residuals, and EOC of FVM for the problem with exact solution taken from the EGM2008 up to degree and order 5

h_{\max}	$\ e_{h_{\max}}\ _{L_2}$	EOC	$\ e_{h_{\max}}\ _{\max}$	EOC $_{\max}$
0.125	9.25506e-05	–	0.000911	–
0.0642	2.39154e-05	2.01	0.000348	1.43
0.0324	8.80662e-06	1.462	0.0001389	1.349
0.0162	2.96979e-06	1.579	4.87918e-05	1.51659
0.00817	9.39478e-07	1.667	1.5969e-05	1.61833

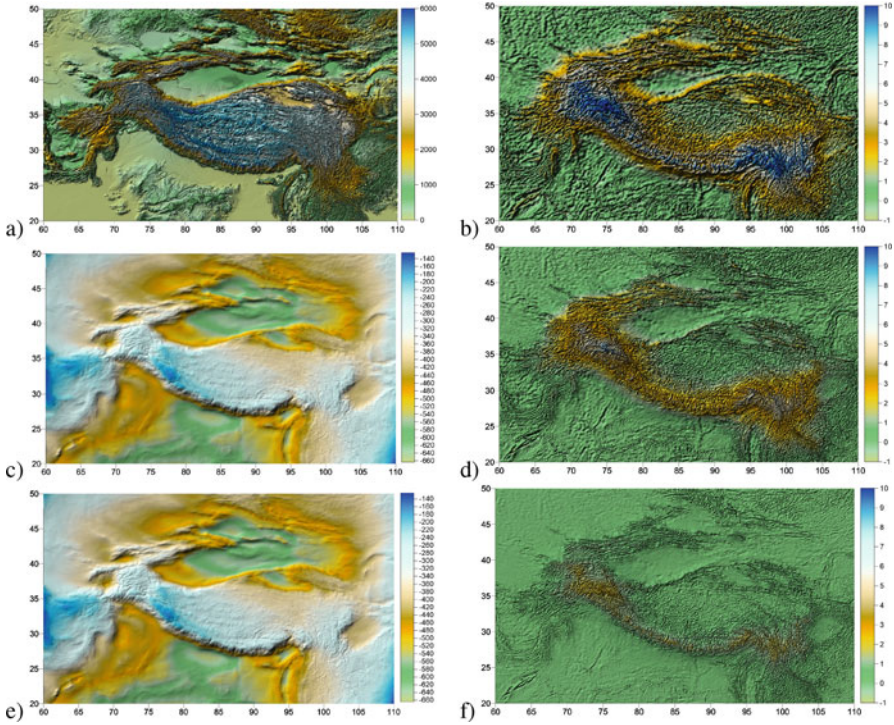


Fig. 17 (a) The Earth's surface topography over the Himalayas (the bottom boundary) [m], (b) the disturbing potential from EGM2008 on the Earth's surface [$m^2 s^{-2}$], (c) the disturbing potential from our FVM solution [$m^2 s^{-2}$], d, e, f) residuals between the EGM2008 and our FVM solution, where grid density is: (d) $501 \times 301 \times 25$, (e) $1001 \times 601 \times 49$, (f) $2001 \times 1201 \times 97$ points [$m^2 s^{-2}$]

Three experiments with different grid densities were performed, namely the grids with the densities $501 \times 301 \times 25$, $1001 \times 601 \times 49$ and $2001 \times 1201 \times 97$ points. They approximately correspond to spacing $0.1^\circ \times 0.1^\circ \times 10$, $0.05^\circ \times 0.05^\circ \times 5$ and $0.025^\circ \times 0.025^\circ \times 2.5$ km.

Figure 17b shows EGM2008 at points on the Earth's topography as the harmonic function that we are reconstructing. The obtained FVM solution for the most dense grid is depicted in Fig. 17c. Residuals between EGM2008 and our FVM solutions on the bottom boundary can be seen in Fig. 17c, d, e. The statistical characteristics of

Table 9 Statistics of residuals between our FVM solution and the EGM2008 in the domain above the Himalayas [m^2s^{-2}]

Resolution	$0.1^\circ \times 0.1^\circ \times 10 \text{ km}$	$0.05^\circ \times 0.05^\circ \times 5 \text{ km}$	$0.025^\circ \times 0.025^\circ \times 2.5 \text{ km}$
Grid density	$501 \times 301 \times 25$	$1001 \times 601 \times 49$	$2001 \times 1201 \times 97$
Min. value	-5.07	-1.68	-0.44
Mean value	1.79	0.87	0.33
Max. value	23.05	11.98	3.90
St. deviaton	2.3	1.09	0.37

the corresponding residuals are summarized in Table 9. It is evident that refinements of the grid leads to higher accuracy of the FVM solution giving better agreement with EGM2008. Standard deviations (STDs) are decreasing from 2.3 to 0.37 m^2s^{-2} ($\sim 2.3 \text{ dm}$ to 3.7 cm) and the maximal values from 23.1 to 3.9 m^2s^{-2} (\sim from 2.3 m to 3.9 dm).

6 Summary

In this chapter we have presented several numerical approaches for solving the oblique derivative boundary value problem based on the boundary element and finite volume methods. Some of these approaches have been applied on uniform and one on nonuniform grids. The presented numerical experiments have confirmed that obtained numerical solutions converge to the exact solutions. Finally we may conclude that presented numerical methods may provide an important basis for solving various geoscientific problems described by partial differential equations.

Acknowledgements This work was supported by Grants APVV-15-0522, VEGA 1/0608/15 and VEGA 1/0714/15.

References

1. Andersen, O.B., Knudsen, P., Berry, P.: The DNSCO8 ocean wide altimetry derived gravity field. Presented at EGU-2008, CityplaceVienna, country-regionAustria (2008)
2. Aoyama, Y., Nakano, J.: RS/6000 SP: Practical MPI Programming. IBM, Poughkeepsie/New York (1999)
3. Baláš, J., Sládek, J., Sládek, V.: Stress Analysis by Boundary Element Methods. Elsevier, Amsterdam (1989)
4. Barrett, R., Berry, M., Chan, T.F., Demmel, J., Donato, J., Dongarra, J., Eijkhout, V., Pozo, R., Romine, C., Van der Vorst, H.: Templates for the Solution of Linear Systems: Building Blocks for Iterative Methods. SIAM, Philadelphia (1994)
5. Bauer, F.: An alternative approach to the oblique derivative problem in potential theory. PhD thesis, Geomatics Group, Department of Mathematics, University of Kaiserslautern. Shaker Verlag, Aachen (2004)
6. Becker, J.J., Sandwell, D.T., Smith, W.H.F., Braud, J., Binder, B., Depner, J., Fabre, D., Factor, J., Ingalls, S., Kim S.H., Ladner, R., Marks, K., Nelson, S., Pharaoh, A., Trimmer,

- R., Rosenberg, J. Von, Wallace, G., Weatherall, P.: Global bathymetry and elevation data at 30 arc seconds resolution: SRTM30 PLUS. *Mar. Geod.* **32**(4), 355–371 (2009)
7. Bitzadse, A.V.: *Boundary-Value Problems for Second-Order Elliptic Equations*. North-Holland, Amsterdam (1968)
 8. Bjerhammar, A., Svensson, L.: On the geodetic boundary value problem for a fixed boundary surface. A satellite approach. *Bull. Geod.* **57**(1–4), 382–393 (1983)
 9. Brebbia, C.A., Telles, J.C.F., Wrobel, L.C.: *Boundary Element Techniques, Theory and Applications in Engineering*. Springer, New York (1984)
 10. Čunderlík, R., Mikula, K., Mojžeš, M.: 3D BEM application to Neumann geodetic BVP using the collocation with linear basis functions. In: *Proceedings of ALGORITHMY 2002, Conference on Scientific Computing, Podbanské*, pp. 268–275 (2002)
 11. Čunderlík, R., Mikula, K., Mojžeš, M.: Numerical solution of the linearized fixed gravimetric boundary-value problem. *J. Geod.* **82**, 15–29 (2008)
 12. Čunderlík, R., Mikula, K.: Direct BEM for high-resolution gravity field modelling. *Stud. Geophys. Geod.* **54**(2), 219–238 (2010)
 13. Čunderlík, R., Mikula, K., Špir R.: An oblique derivative in the direct BEM formulation of the fixed gravimetric BVP. *IAG Symp.* **137**, 227–231 (2012)
 14. Eymard, R., Gallouet, T., Herbin, R.: Finite volume approximation of elliptic problems and convergence of an approximate gradient. *Appl. Numer. Math.* **37**(1–2), 31–53 (2001)
 15. Fašková, Z.: *Numerical methods for solving geodetic boundary value problems*. PhD Thesis, SvF STU, Bratislava (2008)
 16. Fašková, Z., Čunderlík, R., Mikula, K.: Finite element method for solving geodetic boundary value problems. *J. Geod.* **84**(2), 135–144 (2010)
 17. Freeden, W.: Harmonic splines for solving boundary value problems of potential theory. In: Mason, J.C., Cox, M.G. (eds.) *Algorithms for Approximation. The Institute of Mathematics and Its Applications, Conference Series*, vol. 10, pp. 507–529. Clarendon Press, Oxford (1987)
 18. Freeden, W., Gerhards, C.: *Geomathematically Oriented Potential Theory*. CRC press, Taylor & Francis Group, Boca Raton, Florida (2013)
 19. Freeden, W., Kersten, H.: *The Geodetic Boundary Value Problem Using the Known Surface of the Earth*, Veröff. Geod. Inst. RWTH Aachen, 29 (1980)
 20. Freeden, W., Kersten, H.: A constructive approximation theorem for the oblique derivative problem in potential theory. *Math. Methods Appl. Sci.* **3**, 104–114 (1981)
 21. Freeden, W., Michel, V.: *Multiscale Potential Theory (With Applications to Geoscience)*. Birkhauser, Boston (2004)
 22. Freeden W., Nutz H.: On the solution of the oblique derivative problem by constructive Runge-Walsh concepts. In: Pesenson I., Le Gia Q., Mayeli A., Mhaskar H., Zhou D.X. (eds.) *Recent Applications of Harmonic Analysis to Function Spaces, Differential Equations, and Data Science. Applied and Numerical Harmonic Analysis*. Birkhäuser, Cham (2017)
 23. Greengard, L., Rokhlin, V.: A fast algorithm for particle simulation. *J. Comput. Phys.* **73**, 325–348 (1987)
 24. Gutting, M.: *Fast multipole methods for oblique derivative problems*. PhD thesis, Geomathematics Group, Department of Mathematics, University of Kaiserslautern. Shaker Verlag, Aachen (2007)
 25. Gutting, M.: Fast multipole accelerated solution of the oblique derivative boundary value problem. *Int. J. Geomath.* **3**, 223–252 (2012)
 26. Gutting, M.: *Fast Spherical/Harmonic Spline Modeling*. *Handbook of Geomathematics*, 2nd edn., pp. 2711–2746. Springer, Berlin/Heidelberg (2015)
 27. Hartmann, F.: *Introduction to Boundary Elements. Theory and Applications*. Springer, Berlin (1989)
 28. Holota, P.: Coerciveness of the linear gravimetric boundary-value problem and a geometrical interpretation. *J. Geod.* **71**, 640–651 (1997)
 29. Holota, P., Nesvadba, O.: Model refinements and numerical solution of weakly formulated boundary-value problems in physical geodesy. In: *IAG Symposium*, vol. 132, pp. 320–326 (2008)

30. Húska, M., Medřa, M., Mikula, K., Novyzedlák, P., Remeřiková, M.: A new form-finding method based on mean curvature flow of surfaces. In: Handlovičová, A., Minářehová, Z., Ševčovič, D., (eds.) ALGORITMY 2012, 19th Conference on Scientific Computing, Podbanske, 9–14 Sept 2012, Proceedings of Contributed Papers and Posters. ISBN:978-80-227-3742-5. Publishing House of STU, pp. 120–131 (2012)
31. Klees, R.: Boundary value problems and approximation of integral equations by finite elements. *Manuscr. Geodaet.* **20**, 345–361 (1995)
32. Klees, R., van Gelderen, M., Lage, C., Schwab, C.: Fast numerical solution of the linearized Molodensky problem. *J. Geod.* **75**, 349–362 (2001)
33. Koch, K.R., Pope, A.J.: Uniqueness and existence for the geodetic boundary value problem using the known surface of the Earth. *Bull. Geod.* **46**, 467–476 (1972)
34. Laursen, M.E., Gellert, M.: Some criteria for numerically integrated matrices and quadrature formulas for triangles. *Int. J. Numer. Meth. Eng.* **12**, 67–76 (1978)
35. Lehmann, R., Klees, R.: Numerical solution of geodetic boundary value problems using a global reference field. *J. Geod.* **73**, 543–554 (1999)
36. LeVeque, R.J.: *Finite Volume Methods for Hyperbolic Problems*. Cambridge Texts in Applied Mathematics (2002). ISBN:978-0521009249
37. Lucquin, B., Pironneau, O.: *Introduction to Scientific Computing*. Wiley, Chichester (1998)
38. Macák, M., Čunderlík, R., Mikula, K., Minářehová, Z.: An upwind-based scheme for solving the oblique derivative boundary-value problem related to the physical geodesy. *J. Geod. Sci.* **5**(1), 180–188 (2015)
39. Macák, M., Mikula, K., Minářehová, Z.: Solving the oblique derivative boundary-value problem by the finite volume method, In: ALGORITMY 2012, 19th Conference on Scientific Computing, Podbanske, 9–14 Sept 2012, Proceedings of Contributed Papers and Posters, Publishing House of STU, pp. 75–84 (2012)
40. Macák, M., Mikula, K., Minářehová, Z., Čunderlík, R.: On an iterative approach to solving the nonlinear satellite-fixed geodetic boundary-value problem, In: IAGSymp, vol. 142, pp. 185–192 (2016)
41. Macák, M., Minářehová, Z., Mikula, K.: A novel scheme for solving the oblique derivative boundary-value problem. *Stud. Geophys. Geo.* **58**(4), 556–570 (2014)
42. Mantič, V.: A new formula for the C-matrix in the Somigliana identity. *J. Elast.* **33**(3), 191–201 (1993)
43. Mayer-Gurr, T., et al.: The new combined satellite only model GOCO03s. Presented at the GGHS-2012 in Venice (2012)
44. Medřa, M., Mikula, K., Čunderlík, R., Macák, M.: Numerical solution to the oblique derivative boundary value problem on non-uniform grids above the Earth topography. *J. Geod.* **92**(1), pp 1–19 (2017)
45. Meissl, P.: *The use of finite elements in physical geodesy*. Report 313, Geodetic Science and Surveying, The Ohio State University (1981)
46. Mikula, K., Remeřiková, M., Sarkóci, P., Ševčovič, D.: Manifold evolution with tangential redistribution of points. *SIAM J. Sci. Comput.* **36**(4), A1384–A1414 (2014)
47. Mikula, K., Ševčovič, D.: A direct method for solving an anisotropic mean curvature flow of planar curve with an external force. *Math. Methods Appl. Sci.* **27**(13), 1545–1565 (2004)
48. Minářehová, Z., Macák, M., Čunderlík, R., Mikula, K.: High-resolution global gravity field modelling by the finite volume method. *Stud. Geophys. Geo.* **59**, 1–20 (2015)
49. Miranda, C.: *Partial Differential Equations of Elliptic Type*. Springer, Berlin (1970)
50. Nesvadba, O., Holota, P., Klees, R.: A direct method and its numerical interpretation in the determination of the gravity field of the Earth from terrestrial data. In: IAG Symposium, vol. 130, pp. 370–376 (2007)
51. Pavlis, N.K., Holmes, S.A., Kenyon, S.C., Factor, J.K.: The development and evaluation of the Earth gravitational model 2008 (EGM2008). *J. Geophys. Res.* **117**, B04406. <https://doi.org/10.1029/2011JB008916> (2012)
52. Schatz, A.H., Thomée, V., Wendland, W.L.: *Mathematical Theory of Finite and Boundary Element Methods*. Birkhauser Verlag, Basel/Boston/Berlin (1990)

53. Shaofeng, B., Dingbo, C.: The finite element method for the geodetic boundary value problem. *Manuscr. Geod.* **16**, 353–359 (1991)
54. Sleijpen, G.L.G., Fokkema, D.R.: Bicgstab (l) for Linear Equations Involving Unsymmetric Matrices with Complex Spectrum. <http://dspace.library.uu.nl/handle/1874/16827> (1993)
55. Zhao, K., Vouvakis, M., Lee, J.-F.: The adaptive cross approximation algorithm for accelerated method of moment computations of EMC problems. *IEEE Trans. Electromagn. Compat.* **47**, 763–773 (2005)